JOURNAL OF PETROLOGY | VOLUME 45 | NUMBER 6 | PAGES 1181–1208 | 2004 | DOI: 10.1093/petrology/egh010

Deep and High-temperature Hydrothermal Circulation in the Oman Ophiolite—Petrological and Isotopic Evidence

D. BOSCH[1]*, M. JAMAIS[1], F. BOUDIER[1], A. NICOLAS[1], J.-M. DAUTRIA[1] AND P. AGRINIER[2]

[1]LABORATOIRE DE TECTONOPHYSIQUE, UMR 5568 CNRS/UM2, UNIVERSITÉ MONTPELLIER II, PL. EUGÉNE BATAILLON, 34095 MONTPELLIER CEDEX 5, FRANCE

[2]LABORATOIRE DE GÉOCHIMIE DES ISOTOPES STABLES, IPG-PARIS VII, 4 PLACE JUSSIEU, F-75252 PARIS CEDEX 05, FRANCE

RECEIVED NOVEMBER 28, 2001; ACCEPTED DECEMBER 5, 2003

A systematic search for evidence of high-temperature hydrous alteration within the gabbros of the Samail ophiolite (Oman) shows that most of the gabbros have been affected by successive stages of alteration, starting above 975°C and ending below 500°C. Sr and O isotopic analyses provide constraints on the nature and origin of the fluids associated with these alteration events. Massive gabbros, dykes and veins and their associated minerals depart from mid-ocean ridge basalt (MORB)-source magma signatures ($^{87}Sr/^{86}Sr$ >0·7032 and depleted $\delta^{18}O$ <6‰). These isotopic characteristics identify seawater as the most likely hydrothermal contaminant. Samples affected by low-temperature alteration during greenschist-facies metamorphism are characterized by high water/rock ratios (>10). A second group of samples, including massive gabbros and high-temperature dykes and veins, is characterized by lower water/rock ratios, in the range of 3–5. These samples display a high-temperature hydrothermal alteration related to seawater ingression. The main fluid channels may be sub-millimetre-sized microcracks with a dominantly vertical attitude, which constitute the recharge hydrothermal system, whereas the dykes and veins represent the discharge part. This model requires that these dykes have been generated by hydration of the crystallizing gabbros via seawater penetration, near the internal wall of the magma chamber.

KEY WORDS: *hydrothermal systems; Oman ophiolite; Sr and O isotopes; gabbros and massive dykes*

INTRODUCTION

Hydrothermal circulation near fast-spreading oceanic ridges is typically a greenschist-facies, low-temperature (LT), system (T < 450°C), which operates at the ridge axis down to the base of the sheeted dyke complex and penetrates the entire crust once it has drifted away from the ridge axis (Nehlig & Juteau, 1988; Wilcock & Delaney, 1996; Juteau *et al.*, 2000). The existence of a simultaneous deeper and higher-temperature hydrothermal system, also active at the ridge, was first suspected when Gregory & Taylor (1981), on the basis of oxygen isotope data, and Lanphere (1981) and McCulloch *et al.* (1981), on the basis of strontium isotope data, proposed seawater contamination at high temperatures (HT) of the lower gabbros of the Oman ophiolite.

More recently, petrological studies of the upper gabbros drilled in the fast-spreading crust exposed in the Hess Deep during Ocean Drilling Program (ODP) Leg 147 (Mevel *et al.*, 1996) have revealed that solid-state reactions in hydrothermal veins occurred at 700–750°C, pointing to the existence of hydrothermal circulation at amphibolite-facies conditions within this section of oceanic crust. Manning *et al.* (2000) conducted a similar study of the gabbros from one section in the Nakhl massif of the Oman ophiolite (Fig. 1). They calculated temperatures ranging from 700°C in the uppermost gabbros to 825°C in the deepest gabbros at the Moho. Kawahata

*Corresponding author. E-mail: bosch@dstu.univ-montp2.fr

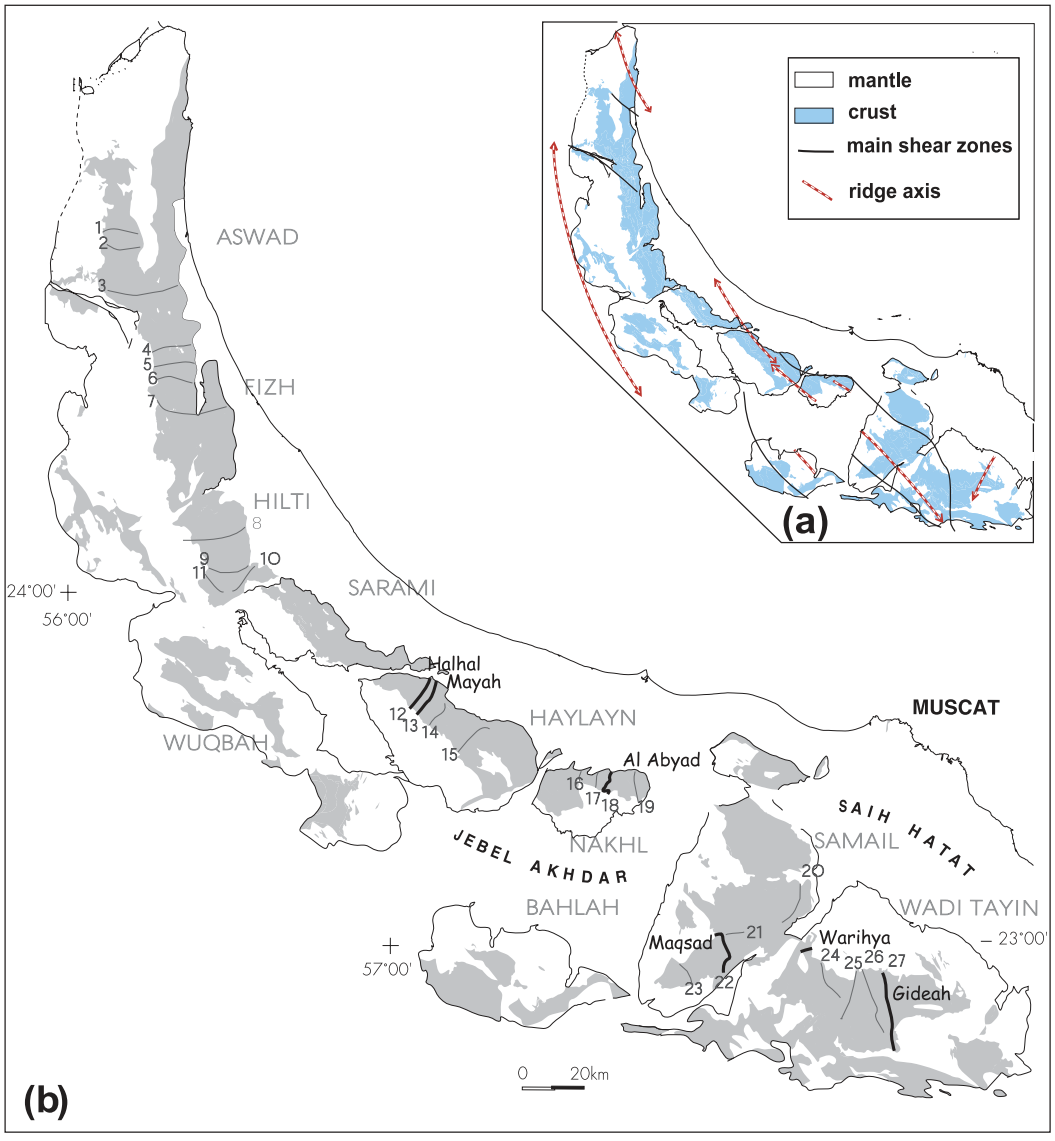

Fig. 1. (a) Simplified map of the Oman–UAE ophiolite including the inferred location of the palaeo-ridge axes and main shear zones [modified from Nicolas *et al.* (2000)]. (b) Simplified map of the Samail ophiolite. Thin numbered lines represent the log-sections of Fig. 4, along wadis where alteration facies have been studied. Bold lines are the wadi sections selected for detailed petrological and geochemical work in this study.

et al. (2001), on the basis of a Sr isotope study of the crustal unit in the Fizh massif of northern Oman, found a rise in the temperature of hydrothermal alteration from low greenschist facies in the basalts to amphibolite-facies conditions in the gabbros.

Boudier *et al.* (2000) have also suggested that seawater could contaminate the lower gabbros during their crystallization, as recorded by the crystallization of gabbronorites in place of olivine gabbros. This contamination at very high temperatures (VHT), possibly as high as 1200°C, is restricted to those parts of the Oman palaeo-ridge that display evidence of ridge-related tectonic activity and the seawater contamination was attributed to this particular tectonic setting.

Improved seismological modelling of fast-spreading ridges at the East Pacific Rise axis at 9°30′N has suggested that there may be significant narrowing of the low-velocity zone (LVZ) below the melt lens (Dunn *et al.*, 2000), with respect to earlier models. This narrowing was explicitly ascribed by Dunn *et al.* to the existence of deep high-T hydrothermal circulation at modern oceanic ridges. This raises the question of the definition of what should be considered as the magma chamber below a mid-ocean ridge. On the basis of extensive studies of the Samail ophiolite, Nicolas *et al.* (1988) have shown that the magma chamber was tent-shaped in three dimensions, extending to the base of the crust, consistent with the shape of the LVZ found below modern ridges. Hence the

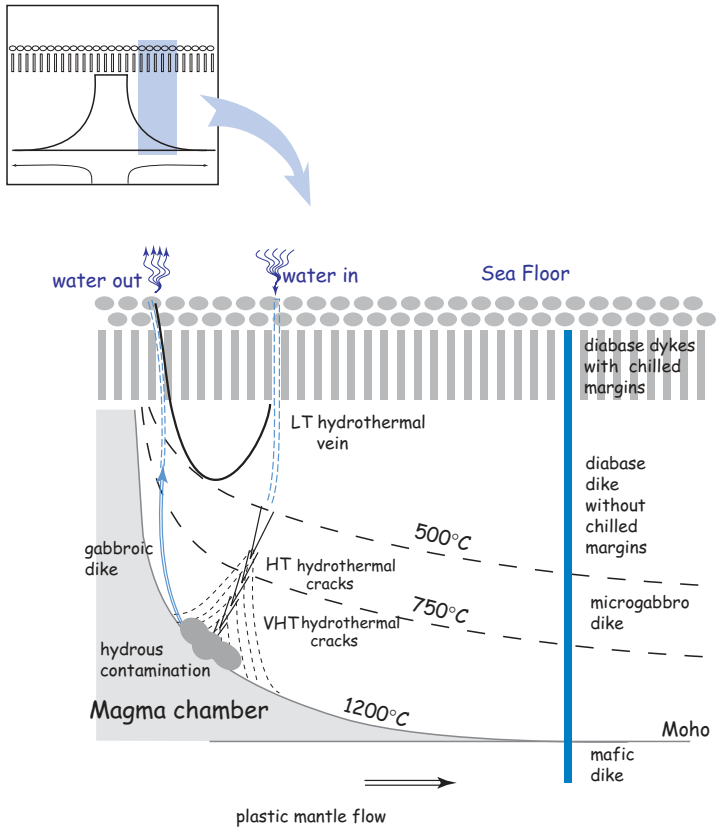

Fig. 2. Scheme of hydrothermal circulation near the limit of the magma chamber, below the fast-spreading ridge. The downgoing seawater flow fills the porous network created by microcracks down to the magma chamber where it reacts with the crystallizing melt; it surges back towards the seafloor along a system of hydrous gabbroic dykes. Modified from Nicolas *et al.* (2003).

magma chamber is not restricted to the perched axial melt lens that is present just below the sheeted dyke complex of fast-spreading ridges (Detrick *et al.*, 1987), because in spite of its very low melt fraction, the LVZ is still deforming as a mush (Nicolas & Ildefonse, 1996).

Building on the previous work of MacLeod & Rothery (1992) and Nehlig *et al.* (1994), Nicolas *et al.* (2001) have recently published a structural map of the greenschist-facies hydrothermal veins throughout the Samail ophiolite. This confirms that the LT veins penetrate the entire crust and are dominantly aligned parallel to the sheeted dyke complex. Subsidiary preferred orientations are related to changes in the stress field during the dying activity of the palaeo-ridge system (Nicolas *et al.*, 2000).

In a companion paper to the present study, Nicolas *et al.* (2003) described a complete transition from these LT hydrothermal veins to gabbroic dykes, which suggests the possibility of seawater-related hydrous melting of the gabbros or entry of seawater into the partially molten magma chamber. Previously, these gabbroic dykes, which are fairly common in the Oman gabbros, were interpreted as late crystallization products from the LVZ magma chamber (Pallister & Hopson, 1981) or as melt conduits related to its magmatic activity (Kelemen *et al.*, 1997; Kelemen & Aharonov, 1998). If the magma that produced these gabbroic dykes originated within the magma chamber, the water should also have an internal origin, the source being either the mantle or the melt lens. In the latter case, contamination by seawater is possible when hydrated diabase, from the overlying sheeted dyke complex, is stoped in the melt lens, remelted and dewatered during subsequent subsidence through the magma chamber.

Alternatively, the gabbroic dykes could result from fractures external to the magma chamber driving seawater to great depth. In the physical model proposed by Nicolas *et al.* (2003), the gabbroic dykes are generated by hydrous melting and represent the discharge system of the high-temperature hydrothermal circulation reaching the inner margin of the magma chamber (Fig. 2). The recharge system is formed by a microcrack network controlled by the anisotropy of thermal expansion, and operating at falling temperatures below 1200°C, within a distance of ~10 km from the spreading axis.

The available geochemical evidence, bearing on the hydrothermal alteration of the gabbros (Gregory & Taylor, 1981; Lanphere, 1981; McCulloch *et al.*, 1981; Kawahata *et al.*, 2001) favours a seawater origin, with seawater/rock ratios ranging from one (Gregory &

Taylor, 1981) to as high as nine (Kawahata *et al.*, 2001). Oxygen isotope data (C. Lecuyer, personal communication, 1990) on mafic dykes emplaced in the peridotites at 1 km below the Moho suggest a dual source of hydration for the gabbros, in which clinopyroxenes have a mantle signature but associated plagioclase and brown hornblende show evidence of seawater contamination. This dual source was not ruled out by Benoit *et al.* (1996) in their Sr isotope study of similar dykes injected into the mantle section. Rare earth element partition coefficients in clinopyroxene, plagioclase and amphibole were used by the above workers to constrain the temperature of seawater contamination at the gabbro solidus.

Thus, there is growing evidence that supports a deep penetration of high-T hydrothermal fluids into the oceanic crust at the ridge axis. We have conducted a systematic study of the gabbros in the Samail ophiolite, and along selected wadi sections (Fig. 1) in the hydrated gabbroic dykes that cross-cut them, looking for traces of HT alteration.

This study combines microtextural and petrological observations, thermometric determinations and O–Sr isotope data on the same gabbroic dykes and surrounding gabbros, selected with a view to determine the origin of hydrous fluid contamination. These results have important consequences for thermal modelling of the oceanic crust near fast-spreading ridges and on the budget of chemical exchanges between the oceanic crust and seawater.

HYDROUS ALTERATION OF PRIMARY MINERALS IN THE GABBRO SECTION

The penetrative alteration of the gabbro section has been studied on the basis of an extensive thin-section collection, which covers the entire ophiolite. The studied gabbros range from the root zone of the sheeted dyke complex down to the Moho and the Moho transition zone (MTZ). From the 500 specimens that have been screened, those sites involved in tectonic complexities, such as the end of segments or tips of propagating rifts (Fig. 1), have been rejected, thus reducing the number of studied areas and the number of fully characterized specimens to 414, representative of standard gabbros at a fast-spreading palaeo-ridge. In this study we mainly focus on hydrous alteration of olivine and clinopyroxene, as these are the minerals most affected by high-T alteration (above 800°C), although plagioclase is stable down to this temperature.

Alteration facies

The following types of hydrous parageneses in the gabbros have been distinguished from highest to lowest temperatures.

(1) Orthopyroxene partial coronas between olivine and plagioclase, which may be associated with the first appearance of brown pargasite blebs inside clinopyroxene and development of pargasite between olivine and plagioclase or clinopyroxene and plagioclase (Fig. 3a). The brown pargasite locally grades into a greenish magnesiohornblende. Although the orthopyroxene coronas could be assigned to a late magmatic stage, we interpret them as reactive, (a) being restricted to the contact between olivine and plagioclase, thus postdating the crystallization of plagioclase, (b) being locally relayed by kelyphitic coronas that spread into plagioclase microcracks (Fig. 3b), as microphases among which diopside and low-titanium pargasite have been identified. We infer that these reactions are related to an oxygen fugacity increase as a result of seawater input. Based on experiments at 2 MPa pressure, Koepke *et al.* (2003) have constrained the equilibrium olivine–orthopyroxene at low water content at 1030°C, and 950°C at higher water content, the limit at which amphibole is stabilized. By reference to this experimental work, we estimate that the temperature of equilibration for these reactions, referred to here as VHT (very high temperature) hydrous alteration, was between 900 and 1000°C.

(2) Chlorite and pale amphibole coronas between olivine and plagioclase (Fig. 3d). The coronas are composed of successive rims of clino-amphibole (tremolite) + magnetite, Mg-chlorite (clinochlore) and a fringe of ortho-amphibole against plagioclase. As described above, these minerals are associated with blebs of brown to greenish amphibole inside the pyroxenes (Fig. 3c). Depending on the degree of alteration, olivine is surrounded by a thin film of amphibole and chlorite or is totally replaced by an assemblage of tremolite + magnetite + plagioclase An_{91} (+ talc), surrounded by chlorite (Fig. 3e). The evolution of the first assemblage to Mg-chlorite indicates temperatures above 700°C, the upper breakdown of Mg-chlorite at 2 kbar (Chernosky *et al.*, 1988). The development of pargasitic amphibole replacing clinopyroxene implies temperatures between 550 and 900°C (Liou *et al.*, 1974; Spear, 1981). We refer to these as HT (high temperature).

(3) Iddingsite, partly or totally replacing olivine, independently of orthopyroxene or chlorite–amphibole coronas and any significant HT alteration in clinopyroxene (Fig. 3f). Observations in thin sections show that the chlorite–amphibole coronas develop before the iddingsite alteration.

(4) Lizardite alteration of olivine, forming the familiar mesh structure. This is always accompanied by saussurite in plagioclase. This alteration takes place below 500°C and is here referred to as LT (low temperature) hydrous alteration. It is only at this stage that plagioclase shows signs of alteration.

These various hydrous alteration facies are commonly observed superimposed in a set of thin sections from a

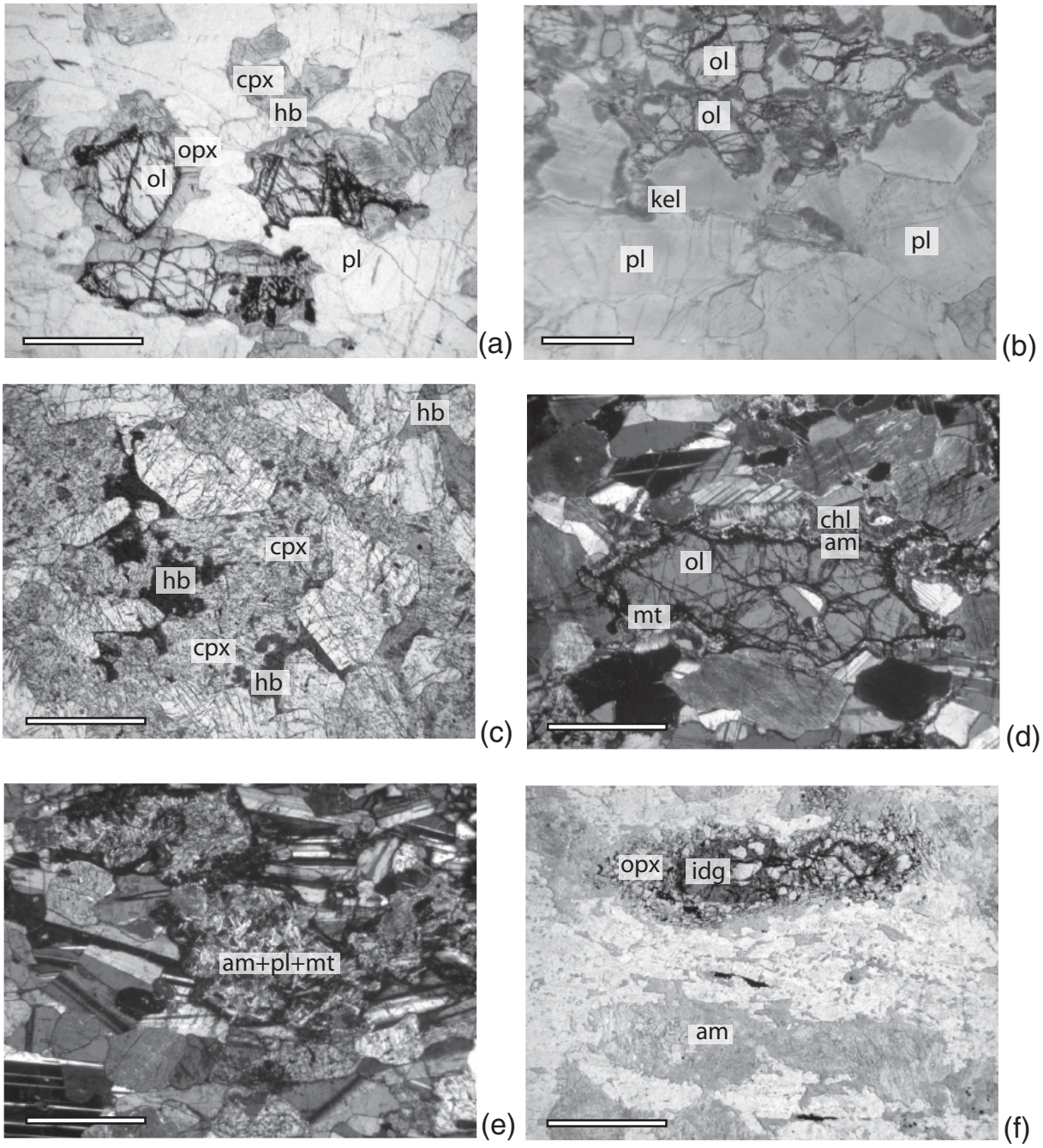

Fig. 3. Hydrothermal alteration in the gabbros (scale bar represents 1 mm). (a) VHT alteration, marked by orthopyroxene (opx) coronas at the contact of olivine (ol) and plagioclase (pl), and pargasitic hornblende (hb) at the contact of olivine and clinopyroxene (cpx) (sample 94 MA2). (b) Kelyphite (kel) coronas around olivine, and cloudy plagioclase as a result of silicate and fluid inclusions. Silicate inclusions tend to be localized at grain boundaries and along microcracks (sample 94 MA2). (c) VHT alteration marked by brown amphibole (hb) alteration of clinopyroxene in an upper gabbro. (d) HT alteration marked by chlorite (chl) (external rim), and pale amphibole (am) and magnetite (mt) (internal rim) coronas around olivine. (e) Total replacement of olivine by an assemblage of tremolite (am) + magnetite (mt) + plagioclase (pl). (f) Total replacement of olivine by an iddingsitic mixture (idg) inside a VHT recrystallized corona of a mosaic of orthopyroxene.

single outcrop and even in a single thin section. As a rule, the orthopyroxene reactions are more penetrative, being homogeneously distributed from the scale of a thin section to that of several thin sections made from a given outcrop. The distribution of chlorite–amphibole coronas is similar, although they can be restricted to the margins of microcracks filled by the same minerals, which have been interpreted as the channels that carried the

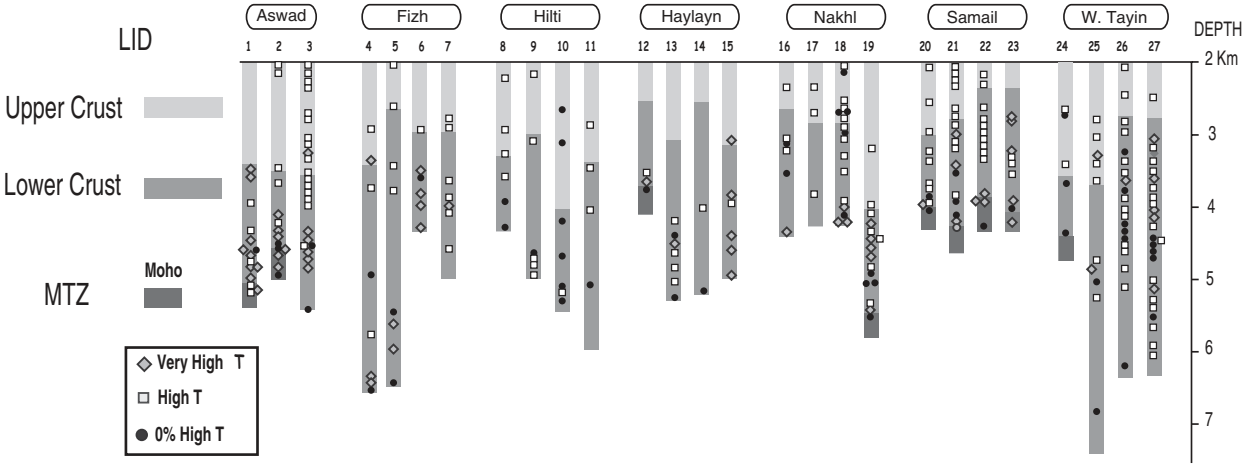

Fig. 4. Depth of penetration of hydrothermal circulation in gabbros along the wadi sections numbered in Fig. 1, referring to alteration facies described in Fig. 3. Depths are recorded below the palaeo-seafloor. LID corresponds to the upper crust including sheeted dykes and volcanics.

fluids responsible for the hydrothermal alteration (Nicolas *et al.*, 2003). The iddingsite replacement is typically heterogeneous at the thin-section scale, being preferentially associated with microcracks. Serpentinization also develops from microcracks, but it can pervasively invade the entire thin section. The microcracks are common; approximately 25% of the studied thin sections display one or more. Ignoring the cracks related to LT alteration and considering only the cracks related to the HT hydrothermal alteration, this fraction is still around 20%.

Distribution of high-*T* alteration facies

Figure 4 shows the distribution of alteration facies as a function of depth in the crust along wadi sections through the Oman–UAE ophiolite offering continuous exposures (see details in Fig. 1). Figure 4 excludes the LT facies because, (1) being based on the presence of olivine serpentinization only, throughout our compilation, its distribution is biased by the decreasing amount of olivine upsection, and (2) this study concerns high-temperature alteration processes. Despite the fact that the scale of sampling may exceed the scale of heterogeneity, evidence for both VHT alteration and 'no alteration' increases with depth. Conversely, HT alteration is predominant in the middle and upper parts of the gabbro section. This observation is valid throughout the wadi sections studied, with the exception of the Wadi Tayin massif, which shows no clear gradation with depth.

Figure 5 is another representation of alteration-facies distribution with depth, based on the detailed study of 414 thin sections. The samples are classified according to their level in the gabbro section: sheeted dyke root zone gabbros, upper gabbros, middle gabbros, lower gabbros and Moho gabbros (the Moho gabbros have been grouped together with the gabbro lenses interlayered in the dunites of the MTZ). Values represent the percent of

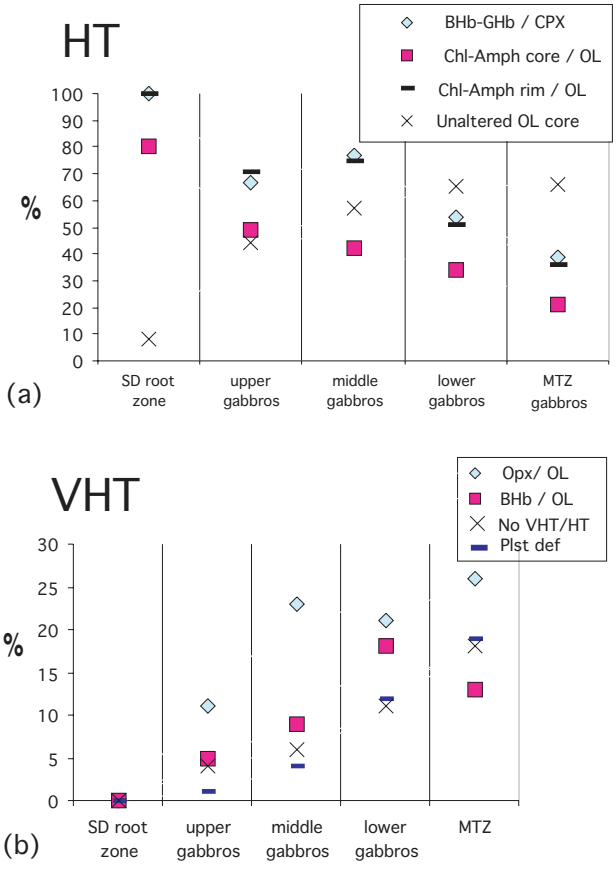

Fig. 5. Compilation of hydrothermal alteration features as a function of depth in the gabbro section. Percentages represent the occurrence of a given type of alteration versus the number of thin sections examined for each selected level: root of the sheeted dykes (SD), upper gabbros, middle gabbros, lower gabbros, MTZ (Moho Transition Zone) gabbros, on a total amount of 414 thin sections (Opx, orthopyroxene; Amph, amphibole; OL, olivine; BHb, brown hornblende; GHb, green hornblende; Chl, chlorite; Plst def, plastic deformation). (a) Distribution of the HT alteration (in %). (b) Distribution of the VHT alteration (in %).

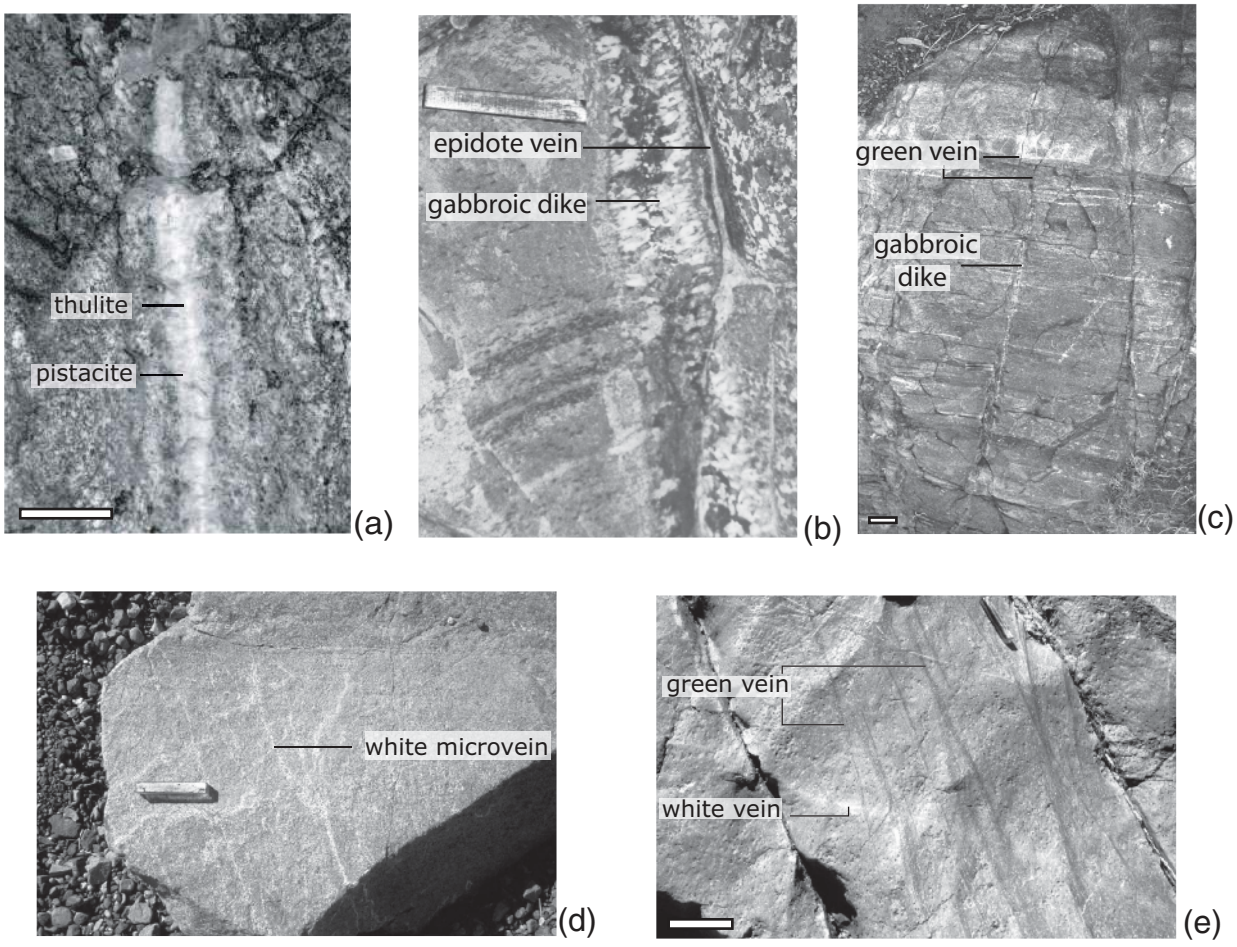

Fig. 6. Field relationships of dykes and veins (scale bar represents 10 cm). (a) Thulite–pistacite vein cross-cutting a foliated gabbro matrix. Reaction margins marked by the development of secondary clinopyroxene (01 OA36b). (b) Comb-like structure in gabbroic dyke. A pink epidote vein follows the margin of the dyke (01 OA15f). (c) Along-strike transition from a gabbroic dykelet to a hydrothermal green amphibole vein. (d) White prehnite vein. (e) Green amphibole vein cross-cut by white prehnite vein.

a given alteration facies as defined previously, out of the total number of thin sections examined for a given level. More refined conclusions can be drawn from this figure.

As seen in Fig. 5a, the HT alteration decreases downwards, whereas it affects most of the upper gabbroic section (sheeted dyke root zone and upper gabbros). The fraction of unaltered olivine cores can be used as an index to estimate the extent of alteration. This index shows that the HT alteration is more penetrative and intense in the upper gabbros, a conclusion already reached by several workers (e.g. Gregory & Taylor, 1981; Stakes & Taylor, 1992; Kawahata *et al.*, 2001). This was also noted by Manning *et al.* (1996*a*, 1996*b*).

Figure 5b shows that the VHT alteration marked by orthopyroxene or brown hornblende coronas around olivine increases with depth. The correlation between the VHT alteration and plastic deformation also suggests that the VHT alteration may coincide with the development of plastic flow at the expense of the magmatic flow, at temperatures just below the solidus. In Fig. 5b, the fraction of gabbros where there is no VHT–HT hydrothermal alteration increases downsection, indicating that the VHT–HT alteration is more localized downsection.

Gabbroic dykes and veins

The occurrence of gabbroic dykes in the layered gabbros of the Samail ophiolite is ubiquitous. We describe gabbroic dykes and sills, either plagioclase–clinopyroxene and brown amphibole-bearing dykes, or microgabbros and amphibolitized dolerite dykes and sills, corresponding to temperatures up to 975°C (see below). Identification of gabbroic dykes in the field is not always straightforward because they may be obliterated by superimposition of greenschist-facies alteration (Fig. 6a). Selective greenschist-facies alteration has frequently been observed, either in the centre of a mafic dyke, or along both margins (Fig. 6b), as well as a continuous transition

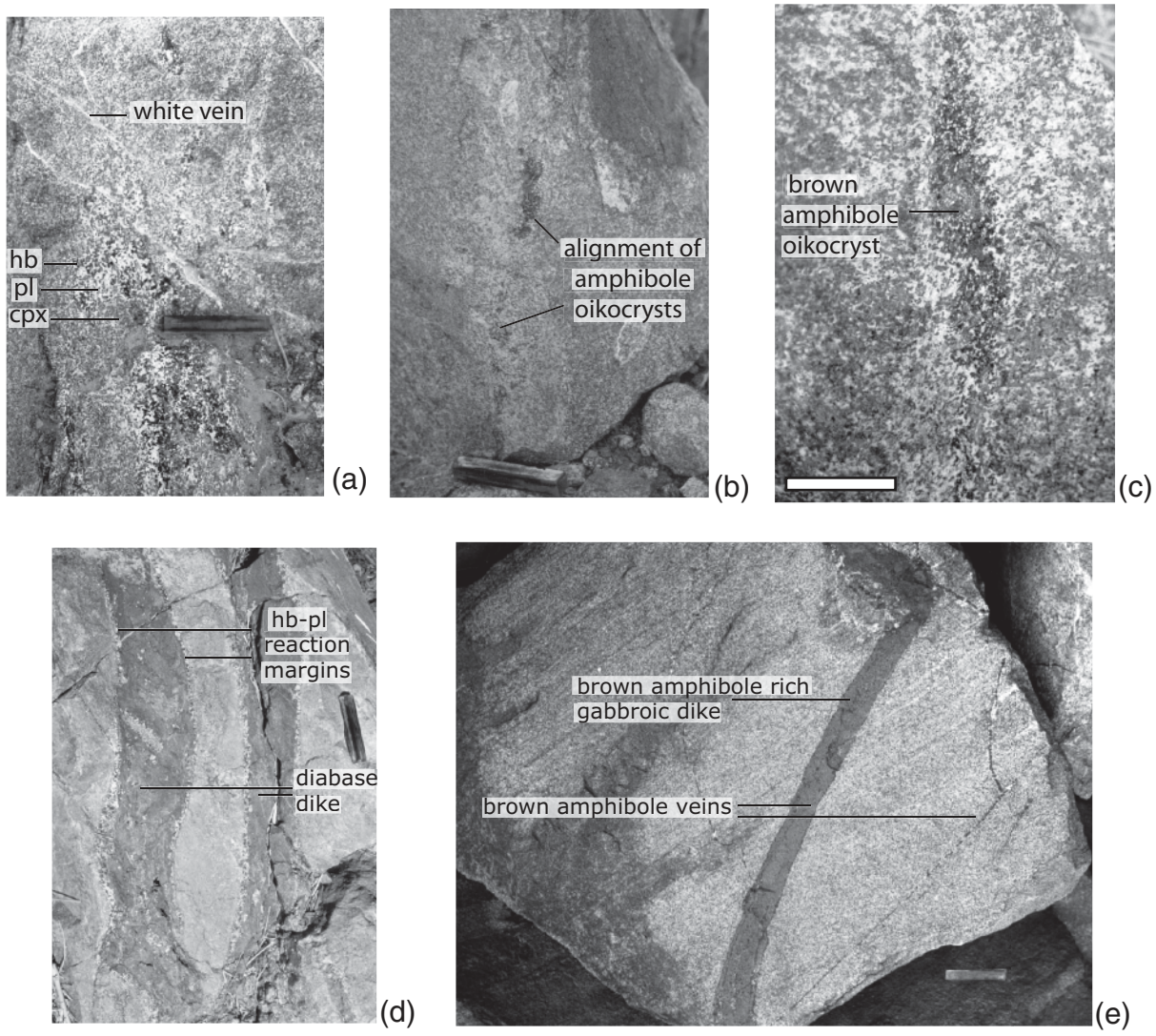

Fig. 7. Field relationships of dykes (scale bar is 10 cm long). (a) Irregular coarse to pegmatitic patches in a foliated gabbro matrix (01 OA42d). (b) Alignment of black amphibole oikocrysts in a foliated gabbro matrix. (c) Local concentration of brown amphibole in a gabbroic dykelet. The plagioclase laths marking the foliation in the enclosing gabbro rotate into parallelism with the gabbroic dykelet. (d) Two diabase dykes assimilating the enclosing layered gabbro, with plagioclase–amphibole reaction margins. (e) Pargasite-rich gabbroic dyke with wall reactions (01 OA19). (Note small pargasite–plagioclase veins.) pl, plagioclase; cpx, clinopyroxene; hb, hornblende.

along a single crack from a mafic dyke to a hydrothermal vein (Fig. 6c). We define hydrothermal veins as cracks filled with greenschist-facies minerals that induce metamorphic reactions in the adjacent country rocks, and gabbroic dykes as planar intrusive bodies produced by the crystallization of magma. Following Nehlig & Juteau (1988), we distinguish low-T greenschist-facies 'white veins' made of prehnite, epidote, chlorite and actinolite (Fig. 6d), and 'green veins' in which a darker green amphibole predominates (Fig. 6e), corresponding respectively to lower (195–410°C) and higher (400–530°C) temperatures (Nehlig & Juteau, 1988).

The gabbroic dykes are typically a few centimetres across, composed of plagioclase, clinopyroxene and brown hornblende. They are coarse-grained to pegmatitic, and commonly display a comb-like structure (Fig. 6b). Although the spacing between the dykes in the field is highly variable, the average is around 10 m. Gabbroic sills grade from clear intrusions to irregular and diffuse pegmatitic gabbro patches, up to a few metres in their larger dimension (Fig. 7a).

The distribution in the field of brownish pargasite, which appears black and glassy in outcrop, is critical in tracing the origin of the gabbroic dykes. It is first observed at any level in the host lower and middle gabbros, as large poikilitic patches (Fig. 7b), locally associated with similarly poikilitic patches of clino- and orthopyroxene (Fig. 7a). These patches contain small aligned tablets of

plagioclase, oriented parallel to the larger plagioclase laths defining the magmatic foliation of the gabbro (Fig. 7c). Clinopyroxene oikocrysts surrounding idiomorphic plagioclase crystals are common in the upper-level gabbros; they mark the end of the magmatic flow and crystallization, growing before the pargasite and orthopyroxene oikocrysts, as shown by their partial replacement by pargasite. Their crystallization marks the transition at suprasolidus conditions from a dry to a wet environment. In the uppermost gabbros, those dykes that are typically altered in the HT hydrothermal facies grade upwards into the so-called 'isotropic' or 'varitextured' gabbros.

The microgabbro and amphibolitized dolerite dykes differ from the typical diabase dykes commonly cutting the gabbro section that have chilled margins, and thus probably intruded enclosing rocks already at temperatures below 450°C. In microgabbro and amphibolitized dolerite dykes, the absence of chilled margins and the development of dioritic reaction margins in the adjacent gabbro (Fig. 7d and e) suggest that they were emplaced in gabbros that were still at temperatures above 750°C (Nicolas *et al.*, 2000).

ANALYTICAL TECHNIQUES

Major and trace elements

Major element compositions were determined by electron microprobe at the University of Montpellier II, using a Camebax SX100. Instrument calibration was performed on natural standards and operating conditions were 20 kV accelerating potential, 10 nA beam current and 30 s counting time.

Rb and Sr concentrations in whole rock and separated mineral fractions were measured by conventional nebulization inductively coupled plasma mass spectrometry (ICP-MS) using a VG Plasmaquad 2 (ISTEEM, Montpellier). Digestion procedures followed those outlined by Ionov *et al.* (1992).

O–Sr isotopes

The samples selected for the detailed study were extracted from gabbroic dykes or veins inside gabbros and cut with a diamond saw into 2–3 cm fragments before being crushed into 0·5–1 cm fragments. For whole-rock analysis, small pieces were further crushed into powder in an agate bowl. For pure mineral analysis, the fragments were crushed with a manual agate mortar. To avoid or minimize the mixing of selected separate minerals with other phases that can bias the results, a strict protocol of mineral selection was applied. A small size fraction of 125–160 μm was used and minerals were first separated using a Frantz isodynamic magnetic separator. Concentrates recovered (cpx, plagioclase, amphibole, epidote) were subsequently purified by careful hand-picking in alcohol under a binocular microscope. At this stage, mineral separates were very pure and only flawless minerals, free of cracks and visible inclusions, were kept for isotopic analyses. To ensure further mineral integrity, these pure mineral separates were ultrasonically washed in dilute 1·5N HCl and rinsed several times with ultra-pure water. This stage potentially removes adsorbed secondary micro-phases. Previous studies (e.g. Lecuyer & Reynard, 1996) demonstrated that pyroxene and amphibole can be intermixed on a very fine scale with other phases (such as a range of amphibole compositions, talc, Fe-oxide). Although this possibility cannot be ruled out, the procedure used in this study makes it unlikely that complex minerals passed through the selection.

Sr isotopic compositions

Approximately 50 mg of whole-rock powder or separated minerals were digested in a Teflon 'bomb' with a mixture of triple distilled 13N HNO_3 and 48% HF with a few drops of $HClO_4$. Two aliquots were separated, one for the determination of Sr isotopic composition and the other for Sr and Rb contents. Sr was separated using an extraction chromatographic method modified from Pin *et al.* (1994). Concentrations were measured by isotope dilution using ^{84}Sr–^{87}Rb mixed spikes. To remove traces of the late low-temperature seawater alteration and to determine the primitive whole-rock Sr isotopic composition, leaching experiments were conducted on a few samples following the procedure described by Bosch (1991). The strontium isotopic compositions of leachates have been analysed in the attempt to check for the leaching efficiency. During these tests, four Sr isotope compositions were measured, which correspond to the unleached sample, the two liquids extracted after acid-leaching steps and the final solid residue. Leaching experiments were conducted in two steps: first, with 6N HCl for 8 min at 70°C; second, with 2·5N HCl for 30 min at 70°C. After leaching, the leachates were evaporated to dryness and the solid residues digested similarly to the unleached samples.

Sr isotopic compositions were measured on a fully automated VG Sector mass spectrometer housed at the University of Montpellier II, except for the Sr isotopic data from the leaching experiments, which have been measured at the Université de Bretagne Occidentale (Brest). To assess the reproducibility and accuracy of Sr isotopic measurements, the NBS 987 standard was run 12 times during this study; the average value was 0·710245 with a precision better than ±0·000010 (2σ). $^{87}Sr/^{86}Sr$ ratios are corrected for mass discrimination by normalizing to a $^{86}Sr/^{88}Sr$ value of 0·1194. Sr total blank concentrations were less than 60 pg. Initial $^{87}Sr/^{86}Sr$

ratios were calculated by correcting the measured ratios for accumulation of ^{87}Sr produced by *in situ* ^{87}Rb radioactive decay since 95 Ma, the assumed age of crystallization of the Oman ophiolite (Hacker, 1994).

Oxygen isotopes

The powdered samples were introduced in Ni tubes under dry air where they were reacted with BrF_5 to form oxygen. Oxygen was separated from other gases by cooling the resulting mixture at liquid nitrogen temperature (77 K) that retained other volatile gases. Oxygen was further purified by trapping it on a cooled 5A molecular sieve at 77 K, then quantified to calculate the yield of the isotopic analyses and finally transferred to the mass spectrometer (Finnigan Mat Delta E) where intensities associated with masses 32 and 34 were measured to determine $\delta^{18}O$. The isotopic composition of a sample is given as $\delta_{sample} = (R_{sample}/R_{standard} - 1) \times 1000$ in per mil unit, where R is $^{18}O/^{16}O$ and the standard is SMOW. Analytical errors on the oxygen isotope ratio are 0·2‰ (2σ).

RESULTS

Seven samples representative of the range of gabbroic dykes and five samples representative of the lower gabbros, two of them representing the margins of gabbroic dykes, were selected for major element, thermometric and Sr–O isotopic analyses (Tables 1–3). These samples originate from wadi sections marked by bold lines in Fig. 1. Wadis Halhal, Mayah, Al Abyad, Warihya and Maqsad structurally belong to a new ridge segment opening in slightly (~1 Myr) older lithosphere; Wadi Gideah is in older lithosphere.

Petrographic and isotopic characteristics of the analysed samples

Olivine gabbro from the MTZ in Maqsad, Samail Massif

Sample 94 MA2 is devoid of low-temperature alteration, and only exhibits the discrete signature of the VHT–HT alteration. The orthopyroxene corona around olivine (Fig. 3a), is relayed by kelyphitic rims at the contact with plagioclase (Fig. 3b). Issuing from these rims are micrometre-sized pale green amphiboles identified as cummingtonite and actinolite, which penetrate the surrounding plagioclase in microcracks 0·04 mm wide or at grain boundaries (Fig. 3b) similar to the microcrack system described by Manning *et al.* (2000). A large number of the plagioclase crystals have a cloudy core as a result of the concentration of fluid and mineral inclusions, among which diopside has been identified during microprobe analysis. Olivine cores are free of serpentine, but they are largely oxidized along a microcrack network. Orthopyroxene coronas have a Mg_{Opx} number of 78–79, slightly higher than in the primary olivine cores with Mg_{Ol} number of 74–75. The magmatic clinopyroxene is totally fresh, and probably not in equilibrium with the reactive orthopyroxene. This sample has the lowest $^{87}Sr/^{86}Sr$ initial ratio of the studied whole rocks (0·70322), identical to coexisting clinopyroxene (0·70324) and plagioclase (0·70322). This observation suggests the lack of a late superimposed LT hydrothermal alteration, as it is very unlikely that an LT hydrothermal event could have totally equilibrated the Sr isotopic compositions of primary minerals such as plagioclase and clinopyroxene. Moreover, the whole rock (WR), clinopyroxene and plagioclase have similar initial Sr isotopic ratios despite very different Sr contents. Accordingly, this ratio is thought to reflect the signature acquired during the crystallization of these minerals and is higher than the Oman mantle Sr isotopic value (McCulloch *et al.*, 1981). The $\delta^{18}O$ values of the WR (5·0‰) and plagioclase (4·8‰) are distinctly lower than primary magmatic values. Indeed, in normal mid-ocean ridge basalts (MORB) the WR $\delta^{18}O$ value is $5{\cdot}7 \pm 0{\cdot}2$‰, with a corresponding plagioclase $\delta^{18}O$ ranging from 5·5‰ to 6·2‰ (Javoy, 1980; Gregory & Taylor, 1981).

Lower gabbro from Wadi Wariyah, Wadi Tayin Massif

Sample 97 OA128b belongs to a layered sequence in the lower gabbro series, injected by anorthositic sills. The sample was collected at the tip of one of these sills, between layers enriched in clinopyroxene. The gabbro is composed of 60% plagioclase and 40% clinopyroxene. Despite the absence of olivine, the WR has a relatively high Mg content (Table 3). A series of low-T (prehnite) microveins, 0·1 mm thick, cross-cut the gabbro perpendicular to the layering and foliation. The margins of the veins are devoid of alteration. This gabbro has the same Sr isotopic composition as 94 MA2. Nevertheless, the WR and associated plagioclase have Sr isotope signatures (0·70333 and 0·70328) lower than the coexisting clinopyroxene (0·70422). The Sr contents of the WR, plagioclase and clinopyroxene are 127 ppm, 120 ppm and 20 ppm, respectively, thus making the clinopyroxene more sensitive to late-stage contamination. Clinopyroxene and plagioclase oxygen isotope compositions (5·23 and 4·14‰, respectively) are also lower than typical mantle values. Similar to the previous sample, alteration, at high temperature, by a low $\delta^{18}O$ and high $^{87}Sr/^{86}Sr$ fluid is required to explain such characteristics.

Amphibole gabbro patch, Wadi Gideah, Wadi Tayin Massif

Sample 01 OA41d2 is from a laminated gabbro composed of millimetre-sized layers of clinopyroxene and plagioclase. Anatectic patches (Fig. 7a) bordering anorthositic layers are formed of coarse-grained

Table 1: Location of the analysed samples and summary of their petrographic and Sr–O isotopic characteristics

Sample name	Site	Location in gabbroic section	Type of rock	Distance to Moho (km)	Paragenesis	Alteration	$^{87}Sr/^{86}Sr$ initial[1]	$\delta^{18}O$ (‰)[2]
94 MA2	Maqsad	From MTZ	Layered gabbro	0	Olivine (Mg no. 74–75)[3]	OPX coronas (Mg no. 78–79)	WR = 0·70322	WR = +4·95
					CPX	Pale green Am (cum/act)	CPX = 0·70324	n.d.
					Plagioclase (An_{65-80}),[4] inverse zoning	No low-*T* alteration	Pl = 0·70322	Pl = +4·79
					Solid/fluid inclusions in Pl			
97 OA128b	Wadi Waryiah	From lower gabbro	Layered gabbro	1	CPX	Low-*T* alteration	WR = 0·70333	n.d.
					Plagioclase (An_{85-87})	Prehnite microveins	CPX = 0·70422	CPX = +5·23
							Pl = 0·70328	Pl = +4·14
01 OA41d2	Wadi Gideah	From upper gabbro	Gabbro patch in laminated gabbro	3·6	CPX recrystallized	Black pargasitic honblende	WR = 0·70351	WR = +4·80
					Plagioclase idiomorphic		CPX = 0·70378	n.d.
					(An_{57-87}), normal zoning		Pl = 0·70426	Pl = +5·04
							Hbd = 0·70355	n.d.
01 OA19a & d	Wadi Waryiah	In layered gabbro	Gabbroic dyke	0·1	Olivine	OPX poikilitic	WR = 0·70341	WR = +5·67
					CPX	Black pargasite	Hbd = 0·70324	Hbd = +2·87
					Plagioclase (An_{73-95})	Hornblende poikilitic	Pl = n.d.	Pl = +10·09
						Hematite	WR = 0·70418	n.d.
						Green Mg-hornblende		
						Act. hornblende		
						Epidote		
02 OA90b	Wadi Al-Abyad	In layered gabbro	Dioritic dyke	0·15	Green Mg-hornblende		Hbd = 0·70427	Hbd = +2·39
					Plagioclase (An_{83-87})		Pl = 0·70387	Pl = +4·98
					Solid/fluid inclusions in plagioclase			
01 OA15f	Wadi Waryiah	In layered gabbro	Comb-textured gabbroic dyke	0·25	CPX idiomorphic	Brown Mg-Hornblende	WR = 0·70458	n.d.
					Plagioclase (An_{95-99}), normal zoning			
02 OA43a	Wadi Mayah	In layered gabbro vein	Green amphibole	1	Pale green Mg-hornblende acicular	Plagioclase (An_{91-97}) in reaction margin	Hbd = 0·70431	Hbd = +3·10
01 OA36b	Wadi Gideah	In layered gabbro	epidosite dyke	2·5	CPX	Epidote	WR = 0·70519	n.d.
					Plagioclase		Ep = 0·70554	n.d.

CPX, clinopyroxene; Pl, plagioclase; OPX, orthopyroxene; Am, amphibole; cum, cummingtonite; act, actinolite; WR, whole rock; Hbd, hornblende; Ep, epidote; n.d., not determined.
[1]$^{87}Sr/^{86}Sr$ initial ratios calculated at 95 Ma (Hacker, 1994). Errors of the measured ratios are indicated in Table 4.
[2]Analytical errors of the oxygen isotope values are 0·2‰ (2σ).
[3]Mg number = atomic Mg/(Mg + Fe).
[4]Percentage of anorthite in plagioclase.

Table 2: Average temperatures (°C, ± 40°C) calculated for plagioclase–amphibole pairs using the geothermometer of Holland & Blundy (1994)

	Pargasite		Magnesio-hornblende	
	rim	core	rim	core
01 OA41d2	878	953	—	—
01 OA19a	935	974	825	869
01 OA19d	890	933	789	—
02 OA37b	—	—	816	849
02 OA90b	—	—	859	833

(millimetre-sized) recrystallized clinopyroxene largely altered to light green magnesio-hornblende, and idiomorphic plagioclase. Locally, primary black pargasitic hornblende develops, including idiomorphic normally zoned plagioclase (Table 4). This gabbro exhibits similar $^{87}Sr/^{86}Sr$ ratios for the WR and pargasite (0·70351 and 0·70355, respectively). These values are interpreted as representative of the melt from which this amphibole crystallized. The clinopyroxene has a slightly higher Sr isotope composition of 0·70378 consistent with the occurrence of the light green Mg-hornblende rim. Plagioclase is significantly more radiogenic (0·70426), related to secondary destabilization evidenced by the idiomorphic habit. The Sr isotope compositions of the liquids extracted from the acid leaching experiments of the WR (L1 and L2) are very similar, 0·70358 and 0·70365, respectively. The $^{87}Sr/^{86}Sr$ ratio of the residue obtained after leaching experiments is 0·70335, lower than both the pargasite and unleached WR. This value can be considered as the unaltered isotopic composition of this sample. The $\delta^{18}O$ values measured for WR and coexisting plagioclase are lower than normal MORB magmatic values. The ^{18}O depletion in the plagioclase can be fairly well explained by high-temperature hydrothermal interaction between an oxygen-depleted fluid and the magma. According to the kinetics of hydrothermal exchange of oxygen (Gregory & Taylor, 1981; Gregory *et al.*, 1989), plagioclase exchanges its oxygen isotopes with the fluid, adjusting readily to the hydrothermal conditions. For high temperatures of exchange with seawater-derived fluids ($\delta^{18}O$ between 0 and +2‰), the magmatic plagioclase will have its primary $\delta^{18}O$ value lowered, whereas the $\delta^{18}O$ value for lower temperatures of exchange (<300°C) will increase. The amplification of the $\delta^{18}O$ shift increases with the intensity of the hydrothermal alteration.

Gabbroic dykes intrusive in lower gabbros from Wadi Wariyah, Wadi Tayin Massif

Gabbroic dykes 01 OA19a and 01 OA19d are intrusive into the lower gabbros. They are 3–4 cm wide, discordant to the foliation of the host gabbros (Fig. 7e), with a sharp margin marked by a brown amphibole fringe. The primary phases in the dykes (Table 1), locally preserved as elongated aggregates of a 0·1 mm grain size mosaic assemblage at the dyke margins, grade to millimetre size in the central part of the dyke. The WR major element composition is Mg enriched compared with the enclosing gabbro (Table 3). Brown pargasitic amphibole oikocrysts make up 50% of the modal composition of the dyke. In dyke 01 OA19a poikilitic orthopyroxene may develop instead of brown amphibole. Finally, green magnesio-hornblende grows either as oikocrysts at the expense of clinopyroxene, or in association with epidote as an alteration product of plagioclase. These low-amphibolite-facies minerals represent the lowest-grade paragenesis recognized in these dykes, and are most developed in sample 01 OA19a. The amphibole composition shows zoning from Ti-rich pargasitic hornblende to magnesio-hornblende and actinolitic hornblende (Fig. 8c), recording progressive cooling of the dyke. The plagioclase composition is extremely heterogeneous (Fig. 8b), varying from An_{95}, a composition similar to that of the plagioclase in the host gabbro (Fig. 8a), to An_{50} for the plagioclase and associated epidote inclusions in the poikilitic actinolitic hornblende. Sample 01 OA19d has an initial $^{87}Sr/^{86}Sr$ ratio slightly higher for the WR (0·70341) than for the pargasite (0·70324). The Sr isotopic ratios of liquids extracted after two steps of WR acid-leaching (L1 and L2) are 0·70357 and 0·70341, respectively, whereas the residue yields a $^{87}Sr/^{86}Sr$ ratio of 0·70327, very close to the pargasite and plagioclase values. The latter is similar to the isotopic composition measured for the massive gabbro 94 MA2 and may be taken as close to the primary magmatic value. This Sr isotopic ratio is more radiogenic than the inferred Oman mantle-source value (McCulloch *et al.*, 1981). The altered part of this sample has a radiogenic Sr isotopic composition (0·70418) related to the low-amphibolite-facies alteration. This gabbroic dyke has seemingly preserved a magmatic whole-rock $\delta^{18}O$ value (5·67‰) but contains by far the highest $\delta^{18}O$ plagioclase (10·09‰) of all the samples analysed. This plagioclase coexists with low $\delta^{18}O$ pargasite (+2·87‰). Similarly high values ($\delta^{18}O_{plagioclase} > 8$) have been previously measured for gabbroic dykes, diabases, sheeted dykes and plagiogranites from the Oman ophiolite (Gregory & Taylor, 1981; Stakes & Taylor, 1992). This 7·2‰ oxygen isotope fractionation between plagioclase and amphibole cannot possibly represent oxygen equilibrium at any plausible temperature. This may be explained by different exchange kinetics for these two minerals at different temperatures at high water/rock

Table 3: Whole-rock major element compositions of massive gabbros and dykes determined by X-ray fluorescence (wt %)

Sample:	94 Ma2	97 OA128b	01 OA41d2	01 OA19d	01 OA19a	01 OA15f	01 OA36b	01 OA36b
Rock type:	Gabbro	Gabbro	Gabbro patch	Gabbroic dyke	Gabbroic dyke	Comb-textured gabb. dyke	Epidosite dyke	Epidosite dyke (margin)
SiO_2	48·30	48·15	47·49	45·24	43·39	47·99	38·9	43·71
Al_2O_3	27·85	20·32	24·38	14·74	12·46	11·92	27·52	16·46
Fe_2O_3	3·28	2·66	4·04	9·81	12·04	5·92	3·81	6·23
MnO	0·03	0·04	0·05	0·14	0·16	0·06	0·08	0·14
MgO	4·05	7·37	4·27	10·31	16·86	13·26	1·87	7·39
CaO	12·89	19·08	14·77	12·35	11·56	16·6	24·71	23·39
Na_2O	2·92	1·23	2·57	2·58	1·11	0·75	0·00	0·13
K_2O	0·00	0·00	0·09	0·06	0·00	0·00	0·00	0·00
TiO_2	0·05	0·17	0·63	2·30	0·64	0·86	0·13	0·42
P_2O_5	0·08	0·07	0·13	0·18	0·09	0·13	0·07	0·10
LOI	0·33	0·76	1·38	2·16	1·61	2·37	2·74	1·90
Total	99·78	99·85	99·8	99·87	99·92	99·86	99·83	99·87

LOI, loss on ignition; gabb., gabbroic.

ratios. This supports the occurrence of two distinct hydrothermal events, one at high temperature and a later stage at lower temperature, responsible for the strong ^{18}O enrichment in the coexisting plagioclase.

Dioritic dyke associated with a diabase dyke in lower gabbros from Wadi Halhal, Haylayn Massif

Sample 02 OA37b belongs to a group of brown amphibole–plagioclase lenses or reaction margins associated with diabase intrusives (Fig. 7d) in lower layered gabbros. Idiomorphic brown hornblende (tschermakite) crystals are elongated in the plane of the dyke representing 80% of the modal composition. They are associated with an interstitial plagioclase matrix. The brown tschermakite has greenish rims. Plagioclase has a cloudy appearance due to micrometre-size fluid inclusions, except along its margins and internal microcracks. Both hornblende and plagioclase exhibit evidence of plastic deformation. The Sr isotopic ratio for the pargasite and plagioclase is 0·70348 and 0·70420, respectively. The pargasite exhibits a Sr signature closest to that of the Oman primary magmatic value (McCulloch *et al.*, 1981). Nevertheless, it is too high to be attributed to an unmodified MORB-source mantle signature. This suggests the addition of an external fluid component in good agreement with the shift of oxygen isotopic composition to a low value (+3·9) suggesting a high-temperature exchange with a low $\delta^{18}O$ fluid. The Sr isotope composition of the plagioclase is significantly higher than that of the coexisting pargasite, probably as a result of the low-temperature alteration.

Dioritic dyke cross-cutting lower layered gabbros in Wadi Al-Abyad, Nakhl Massif

Sample 02 OA90b is a 1 cm thick dioritic dyke cross-cutting the lower layered gabbros. It grades into a green amphibole vein as illustrated in Fig. 6c. The dyke is composed of 2 cm long dark green idiomorphic magnesio-hornblende crystals, growing in the plane of the dyke, and plagioclase concentrated at the margin of the dyke. The plagioclase in the dyke and in the enclosing gabbro contains micrometre-size fluid and mineral inclusions, similar to those observed in sample 94 MA2. The plagioclase and green hornblende have higher Sr isotopic ratios (0·70387 and 0·70427, respectively) and lower $\delta^{18}O$ values (+4·98 and +2·39, respectively) than the normal MORB-source mantle value. As observed for previous samples, this supports interaction with an external fluid component.

Comb-textured gabbroic dykes in the lower gabbros from Wadi Wariyah, Wadi Tayin Massif

Sample 01 OA15f (Fig. 6b) is from Wadi Wariyah and represents a 2 cm wide dyke intruding the lower gabbros. This type of comb-textured dyke developed in the clinopyroxene–plagioclase stability field. It contains large idiomorphic clinopyroxene crystals, which are partially replaced by brownish magnesio-hornblende. The plagioclase is extremely calcic with a slight inverse

Table 4: Major element composition[a] of selected amphiboles, paired with plagioclase compositions used for thermometry

Sample name[1]	Mode[2]	SiO_2	TiO_2	Al_2O_3	Cr_2O_3	FeO	MnO	MgO	CaO	Na_2O	K_2O	Total %	Si	Al^{IV}	Al^{VI}	Ti	Fe^{3+}	Cr	Mg	Fe^{2+}	Mn	Na	K	Ca	X_{An}[3]	T (°C)[4]
01 OA19a																										
Mg-hornblende	core	45·60	2·6	10·78	0·09	8·60	0·15	16·56	12·00	2·12	0·07	96·72	6·552	1·448	0·366	0·083	0·552	0·004	3·409	0·594	0·016	0·611	0·018	1·843	0·903	899
Mg-hornblende	core	47·99	2·63	8·50	0·02	8·97	0·11	16·61	12·10	1·60	0·20	96·36	6·894	1·106	0·334	0·028	0·483	0·002	3·557	0·594	0·014	0·446	0·036	1·862	0·892	834
Mg-hornblende	rim	51·17	2·47	5·96	0·01	7·61	0·14	18·11	12·19	1·03	0·10	96·47	7·257	0·743	0·253	0·016	0·414	0·001	3·828	0·488	0·016	0·284	0·018	1·853	0·894	820
Mg-hornblende	rim	47·50	2·91	9·20	0·04	8·80	0·14	16·46	11·95	1·74	0·08	96·07	6·835	1·165	0·396	0·015	0·506	0·005	3·529	0·552	0·017	0·486	0·015	1·843	0·887	825
Mg-hornblende	rim	49·57	2·69	7·42	0·00	7·99	0·17	18·07	12·02	1·33	0·14	96·88	7·013	0·987	0·261	0·018	0·575	0·000	3·811	0·371	0·020	0·365	0·026	1·821	0·860	831
Mg-hornblende	core	47·83	1·81	8·72	0·03	8·40	0·11	14·48	12·18	1·59	0·08	93·59	6·814	1·186	0·279	0·018	0·644	0·004	3·711	0·357	0·013	0·438	0·015	1·859	0·907	874
Pargasite	rim	42·15	2·49	11·87	0·24	10·07	0·13	13·84	11·43	2·63	0·32	96·61	6·188	1·812	0·242	0·434	0·299	0·028	3·028	0·937	0·016	0·749	0·059	1·797	0·804	972
Pargasite	rim	42·22	2·60	11·86	0·26	10·21	0·11	13·71	11·48	2·53	0·32	96·59	6·201	1·799	0·254	0·429	0·299	0·030	3·001	0·955	0·014	0·720	0·060	1·807	0·803	962
Pargasite	core	42·05	2·63	11·45	0·30	10·19	0·11	13·80	11·47	2·46	0·32	96·46	6·189	1·811	0·175	0·478	0·299	0·035	3·029	0·956	0·014	0·702	0·060	1·809	0·767	974
Pargasite	rim	42·36	2·47	11·90	0·16	9·45	0·13	14·16	11·76	2·49	0·26	95·98	6·239	1·761	0·305	0·366	0·276	0·019	3·109	0·888	0·016	0·710	0·049	1·856	0·818	926
Pargasite	core	42·50	2·91	11·64	0·16	9·84	0·15	14·22	11·41	2·56	0·34	96·69	6·219	1·781	0·227	0·426	0·322	0·018	3·103	0·883	0·018	0·727	0·063	1·789	0·812	974
Pargasite	rim	42·76	2·70	12·03	0·17	9·20	0·12	14·87	11·82	2·44	0·25	96·73	6·224	1·776	0·880	0·335	0·368	0·020	3·226	0·752	0·015	0·689	0·047	1·843	0·841	941
Pargasite	rim	42·13	1·81	13·54	0·16	9·21	0·09	12·77	12·13	2·54	0·32	96·98	6·172	1·828	0·510	0·450	0·000	0·018	2·788	1·129	0·011	0·721	0·059	1·905	0·841	874
01 OA19d																										
Mg-hornblende		49·26	0·47	6·24	0·11	11·46	0·17	15·39	12·21	1·08	0·09	96·48	7·137	0·863	0·202	0·051	0·437	0·013	3·323	0·951	0·021	0·302	0·018	1·896	0·768	771
Mg-hornblende		46·03	2·87	9·32	0·18	9·06	0·17	14·77	12·87	1·93	0·07	97·28	6·672	1·328	0·265	0·313	0·046	0·021	3·191	1·053	0·021	0·542	0·012	1·999	0·758	808
Pargasite		41·89	4·29	11·65	0·08	11·03	0·17	13·52	11·37	2·59	0·17	96·77	6·159	1·841	0·179	0·474	0·345	0·010	2·963	1·012	0·021	0·739	0·032	1·791	0·770	975
Pargasite	rim	42·80	3·40	11·16	0·09	11·01	0·18	13·73	11·67	2·40	0·22	96·67	6·293	1·707	0·226	0·376	0·322	0·010	3·009	1·032	0·022	0·684	0·041	1·839	0·605	880
Pargasite	core	42·58	3·51	11·27	0·06	11·63	0·18	13·51	11·46	2·39	0·22	96·82	6·257	1·743	0·209	0·387	0·391	0·007	2·959	1·039	0·023	0·680	0·042	1·804	0·595	893
Pargasite	rim	42·14	3·93	11·28	0·06	11·71	0·14	13·35	11·33	2·35	0·33	96·62	6·214	1·786	0·174	0·435	0·391	0·007	2·935	1·054	0·018	0·673	0·062	1·790	0·519	901
Pargasite	core	41·56	4·20	12·05	0·06	11·57	0·16	12·51	11·35	2·49	0·27	96·24	6·168	1·832	0·277	0·469	0·276	0·007	2·768	1·160	0·021	0·718	0·052	1·805	0·537	882
Pargasite	core	41·33	4·38	11·49	0·08	11·66	0·15	13·35	11·45	2·64	0·26	96·80	6·105	1·894	0·107	0·487	0·368	0·009	2·941	1·073	0·019	0·757	0·048	1·813	0·537	942
Pargasite		41·08	4·46	12·39	0·12	11·35	0·17	13·13	11·36	2·63	0·15	96·85	6·049	1·951	0·199	0·494	0·368	0·014	2·882	1·030	0·021	0·752	0·027	1·792	0·758	975
02 OA37b																										
Mg-hornblende	rim	45·15	2·60	9·84	0·02	13·28	0·19	14·01	10·87	1·28	0·09	97·33	6·527	1·473	0·203	0·283	0·690	0·002	3·018	0·915	0·023	0·360	0·016	1·683	0·562	828
Mg-hornblende	rim	44·72	2·63	9·88	0·04	13·23	0·21	14·01	10·78	1·33	0·09	96·92	6·494	1·506	0·185	0·287	0·713	0·005	3·032	0·894	0·025	0·374	0·018	1·677	0·593	854
Mg-hornblende	rim	45·68	2·47	9·35	0·04	12·87	0·20	14·10	11·00	1·21	0·11	97·02	6·621	1·379	0·218	0·269	0·598	0·004	3·045	0·962	0·024	0·341	0·020	1·708	0·562	815
Mg-hornblende	core	43·94	2·91	10·87	0·01	12·60	0·23	13·73	10·59	1·42	0·11	96·39	6·410	1·590	0·278	0·319	0·644	0·001	2·985	0·893	0·028	0·401	0·021	1·655	0·710	860
Mg-hornblende	core	44·62	2·70	10·37	0·01	12·66	0·19	14·12	10·58	1·40	0·08	96·73	6·479	1·521	0·253	0·294	0·644	0·001	3·057	0·893	0·023	0·395	0·014	1·646	0·674	851
Mg-hornblende	rim	47·79	1·81	7·96	0·02	12·09	0·25	15·22	11·09	1·00	0·09	97·33	6·866	1·134	0·214	0·196	0·506	0·002	3·260	0·947	0·030	0·280	0·016	1·706	0·503	767
Mg-hornblende	core	45·43	2·49	10·3	0·00	11·99	0·22	14·50	11·14	1·33	0·08	97·48	6·524	1·476	0·267	0·269	0·644	0·000	3·103	0·796	0·027	0·370	0·015	1·715	0·703	838

Sample name[1]	Mode[2]	SiO_2	TiO_2	Al_2O_3	Cr_2O_3	FeO	MnO	MgO	CaO	Na_2O	K_2O	Total %	Si	Al^{IV}	Al^{VI}	Ti	Fe^{3+}	Cr	Mg	Fe^{2+}	Mn	Na	K	Ca	X_{An}[3]	T (°C)[4]
02 OA90b																										
Mg-hornblende	core	48·83	0·38	7·45	0·05	9·39	0·10	17·29	12·24	1·42	0·06	97·21	6·931	1·069	0·041	0·041	0·667	0·005	3·657	0·448	0·011	0·392	0·010	1·862	0·840	856
Mg-hornblende	core	49·49	0·33	7·31	0·03	9·16	0·08	17·40	12·57	1·39	0·05	97·82	6·987	1·013	0·035	0·035	0·552	0·004	3·662	0·530	0·010	0·379	0·009	1·901	0·830	811
Mg-hornblende	rim	48·90	0·40	7·53	0·05	9·32	0·13	17·15	12·22	1·54	0·05	97·29	6·948	1·052	0·042	0·042	0·575	0·006	3·632	0·533	0·015	0·424	0·010	1·861	0·880	869
Mg-hornblende	rim	48·30	0·44	8·00	0·07	9·62	0·10	16·86	12·32	1·61	0·05	97·35	6·873	1·127	0·047	0·047	0·598	0·008	3·576	0·546	0·012	0·443	0·010	1·879	0·870	862
Mg-hornblende	rim	49·12	0·32	7·42	0·10	9·22	0·11	17·36	12·29	1·42	0·06	97·43	6·956	1·044	0·034	0·034	0·621	0·011	3·665	0·471	0·013	0·391	0·010	1·865	0·840	845
02 OA43a																										
Mg-hornblende	rim	48·13	0·40	7·89	0·07	8·60	0·07	17·41	12·19	1·55	0·06	96·36	6·882	1·118	0·212	0·043	0·621	0·008	3·710	0·407	0·008	0·429	0·010	1·867	—	—
Mg-hornblende	rim	50·93	0·35	6·43	0·01	7·59	0·06	18·50	12·24	1·14	0·03	97·28	7·152	0·848	0·217	0·037	0·506	0·001	3·873	0·385	0·007	0·311	0·005	1·841	—	—
Mg-hornblende	rim	50·67	0·14	5·59	0·09	12·33	0·26	15·28	12·44	0·68	0·03	97·50	7·260	0·740	0·204	0·15	0·483	0·010	3·263	0·994	0·032	0·189	0·005	1·909	—	—
Mg-hornblende	rim	50·34	0·13	6·21	0·09	12·49	0·27	15·07	12·51	0·64	0·03	97·78	7·192	0·810	0·240	0·010	0·530	0·010	3·210	0·960	0·030	0·180	0·010	1·910	—	—
Mg-hornblende	rim	45·17	0·60	11·14	0·13	9·88	0·08	15·78	12·33	2·11	0·09	97·31	6·473	1·527	0·355	0·640	0·644	0·015	3·371	0·540	0·010	0·588	0·016	1·892	—	—
Mg-hornblende	rim	49·25	0·32	7·12	0·14	8·45	0·09	17·84	12·32	1·37	0·04	96·95	6·983	1·020	0·170	0·030	0·620	0·020	3·770	0·380	0·010	0·380	0·010	1·870	—	—
Mg-hornblende	rim	48·61	0·32	7·75	0·14	9·75	0·11	16·81	12·57	1·39	0·04	97·50	6·905	1·950	0·203	0·034	0·621	0·016	3·560	0·537	0·013	0·382	0·008	1·914	—	—
94Ma2																										
Anthophyllite		54·98	0·00	2·59	0·01	12·65	0·37	23·35	1·99	0·34	0·00	96·28	7·744	0·256	0·174	0·000	0·161	0·001	4·903	1·330	0·043	0·092	0·001	0·301	—	—
Anthophyllite		55·11	0·00	2·96	0·03	14·09	0·32	23·66	0·63	0·38	0·00	97·18	7·716	0·284	0·205	0·000	0·115	0·003	4·938	1·535	0·038	0·104	0·000	0·095	—	—
Actinolite		48·58	0·04	9·54	0·02	9·60	0·14	17·67	9·99	1·39	0·05	97·02	6·850	0·150	0·435	0·004	0·690	0·002	3·713	0·442	0·017	0·379	0·009	1·510	—	—
Actinolite		51·54	0·04	5·85	0·00	8·90	0·22	20·28	9·30	0·90	0·02	97·05	7·214	0·786	0·178	0·005	0·598	0·000	4·230	0·444	0·026	0·244	0·004	1·395	—	—
01 OA41d2																										
Pargasite	rim	43·05	3·42	10·71	0·08	11·46	0·12	13·50	11·54	1·79	0·67	96·34	6·353	1·647	0·216	0·380	0·368	0·009	2·967	1·046	0·015	0·512	0·127	1·824	0·613	863
Pargasite	rim	42·61	3·54	11·59	0·01	10·59	0·10	13·52	11·87	1·60	0·76	96·19	6·286	1·714	0·302	0·392	0·299	0·001	2·972	1·007	0·012	0·458	0·143	1·877	0·715	844
Pargasite	core	42·54	4·01	11·04	0·06	11·81	0·13	13·21	11·50	2·02	0·39	96·71	6·266	1·734	0·182	0·444	0·368	0·007	2·901	1·087	0·017	0·576	0·073	1·814	0·854	979
Pargasite	rim	43·03	3·85	10·72	0·02	11·70	0·14	13·50	11·95	1·46	0·80	97·17	6·314	1·686	0·168	0·425	0·345	0·002	2·953	1·091	0·018	0·415	0·149	1·878	0·634	852
Pargasite	rim	42·65	3·41	10·60	0·06	11·97	0·14	13·22	11·64	1·83	0·68	96·20	6·332	1·668	0·186	0·381	0·345	0·007	2·926	1·141	0·018	0·528	0·129	1·851	0·620	869
Pargasite	core	42·82	3·67	10·60	0·07	11·93	0·12	13·42	11·44	2·06	0·47	96·60	6·315	1·685	0·158	0·407	0·391	0·008	2·950	1·080	0·016	0·588	0·089	1·808	0·615	899
Pargasite	rim	42·2	3·62	11·10	0·07	11·42	0·16	13·09	11·72	1·79	0·72	95·89	6·282	1·718	0·229	0·405	0·299	0·009	2·905	1·123	0·020	0·518	0·137	1·869	0·715	875
Pargasite	rim	42·42	3·80	11·03	0·06	11·77	0·12	13·00	11·72	1·88	0·69	96·49	6·283	1·717	0·209	0·423	0·299	0·007	2·870	1·158	0·015	0·539	0·131	1·860	0·817	928
Pargasite	rim	42·21	3·64	11·14	0·06	10·73	0·11	13·53	11·68	1·77	0·72	95·59	6·277	1·723	0·229	0·407	0·322	0·007	2·999	1·012	0·014	0·511	0·136	1·862	0·736	883
Pargasite	rim	42·25	3·76	11·03	0·08	10·93	0·15	13·66	11·72	1·85	0·64	96·07	6·257	1·743	0·182	0·418	0·345	0·009	3·016	1·009	0·019	0·531	0·121	1·860	0·766	912
Pargasite	core	42·17	3·96	10·91	0·08	11·10	0·10	13·57	11·49	2·09	0·38	95·85	6·253	1·747	0·159	0·442	0·368	0·010	3·000	1·009	0·013	0·602	0·073	1·826	0·841	981

[a]Major element compositions are in weight percent. —, no plagioclase analysed and no temperature calculated.
[1]Type of amphibole analysed is also indicated.
[2]Blank indicates no zoning observed.
[3]Mole fraction of anorthite in plagioclase adjacent to amphibole grain.
[4]Temperature of equilibrium for the amphibole–plagioclase pair calculated using the Holland & Blundy thermometer (1994). Errors are ±40°C.

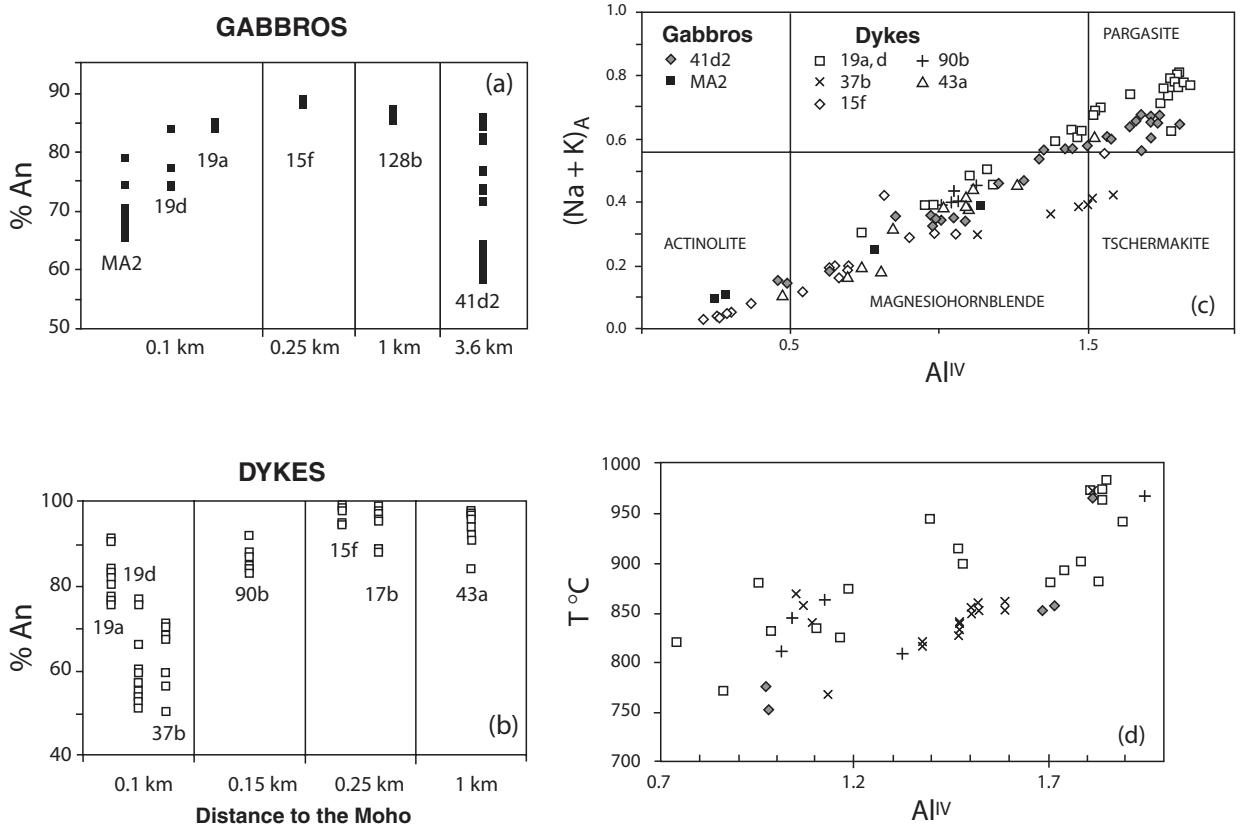

Fig. 8. Plagioclase–amphibole compositions and results of thermometry. (a) and (b) plagioclase compositions in layered gabbros and in dykes, respectively, as a function of distance to the Moho (see text for sample identification); (c) amphibole compositions in layered gabbros and dykes, according to Leake's (1997) nomenclature; (d) equilibration temperatures calculated using the amphibole–plagioclase thermometer of Holland & Blundy (1994), as a function of Al^{IV} content in amphibole [same symbols as in (c)].

zonation from An_{95} to An_{99} from core to rim (Table 1 and Fig. 8a). The WR Sr isotopic ratio of the sample (0·70458) is significantly higher than normal MORB values. This could be related to the overprint of a low-temperature alteration event, consistent with the petrography of the sample.

Green amphibole vein cross-cutting layered gabbros in Wadi Mayah, Haylayn Massif

Sample 02 OA43a belongs to a series of 1 cm thick, green amphibole veins (as in Fig. 6e) cross-cutting the layered gabbros. The veins develop 1·5 cm thick reaction margins in the enclosing gabbro and are exclusively composed of acicular pale green magnesio-hornblende growing perpendicular to the vein margin in a crack-seal mode (Fig. 6f). The reaction margins are composed of uralitized gabbro, marked by the development of the same pale green magnesio-hornblende in an inhomogeneous calcic plagioclase matrix (An_{91-97}). The Sr and O isotopic compositions of this green hornblende (0·70431 and +3·1‰) do not correspond to normal MORB-source mantle values.

Epidosite dyke from Wadi Gideah, Wadi Tayin Massif

Sample 01 OA36b is representative of a series of epidote veins cross-cutting poorly layered gabbros. These 2 cm thick veins are composed of pink thulite in their centre and green pistachite at their margins (Fig. 6a). Their sharp contact with the enclosing gabbro is marked by the development of coarse clinopyroxene crystals altered in the epidote–greenschist facies. This suggests that the epidote vein is replacive in a coarse-grained gabbro dyke. The highest $^{87}Sr/^{86}Sr$ initial ratios of all the samples studied are recorded by the WR and coexisting epidote of this sample (0·70519 and 0·70554, respectively) (Table 5). The Sr content of the WR and associated epidote are also the highest of the present dataset (716 ppm and 764 ppm, respectively). The Sr isotopic composition of this sample is consistent with a greater degree of exchange with a radiogenic component from Cretaceous seawater. It is significantly higher than the value obtained for an epidosite vein from the Wadi Fizh section of the Oman ophiolite [0·70435 with a Sr content of 488 ppm reported by Kawahata *et al.* (2001)] but in good agreement with the average of the greenschist-facies alteration sequence defined by Kawahata *et al.* (2001).

Table 5: Rb and Sr contents, $^{87}Sr/^{86}Sr$ and $\delta^{18}O$ isotopic compositions of whole rocks and mineral separates from samples of massive gabbros, dykes and veins from the Oman ophiolite; also listed are calculated water/rock ratios (W/R) and LOI values

Sample	Rb (ppm)	Sr (ppm)	$^{87}Rb/^{86}Sr$	$^{87}Sr/^{86}Sr$	$(^{87}Sr/^{86}Sr)_i$[1]	$\delta^{18}O$ (‰)	LOI (%)[2]	W/R[3]	$(^{87}Sr/^{86}Sr)L1$[4]	$(^{87}Sr/^{86}Sr)L2$[5]	$(^{87}Sr/^{86}Sr)R$[6]
01 OA41d2											
Whole rock	0·37	179·2	0·006	0·703516 ± 09	0·70351	+4·80	1·38	4·7	0·703587	0·703651	0·703357
Plagioclase	0·25	124·9	0·003	0·704261 ± 22	0·70426	+5·04	—	—			
Pargasite	—	—	—	0·703548 ± 20	0·70355	—	—	—			
Clinopyroxene	0·45	26·0	0·050	0·703845 ± 19	0·70378	—	—	—			
01 OA36b											
Dyke whole rock	0·005	716·4	<0·001	0·705186 ± 17	0·70519	—	2·74	21·9	0·705207	0·705112	—
Epidote	0·003	764·5	0·001	0·705536 ± 12	0·70554	—	—	—			
Wall whole rock	0·05	425·4	0·001	0·704637 ± 09	0·70464	—	1·91	—	0·704945	0·704675	0·704593
02 OA43a											
Green hornblende	0·04	9·8	0·012	0·704323 ± 13	0·70431	+3·10	—	—			
97 OA128b											
Whole rock	0·03	127·4	<0·001	0·703327 ± 17	0·70333	—	0·76	3·7	—	—	—
Plagioclase	0·02	120·4	<0·001	0·703285 ± 09	0·70328	+4·14	—	—			
Clinopyroxene	0·03	20·0	0·004	0·704230 ± 09	0·70422	+5·23	—	—			
01 OA15f											
Whole rock	0·06	107·7	0·002	0·704582 ± 16	0·70458	—	2·37	13·5	—	—	—
01 OA19a											
Whole rock	0·37	130·3	0·008	0·704189 ± 18	0·70418	—	1·61	9·6	—	—	—
01 OA19d											
Whole rock	0·58	203·2	0·008	0·703423 ± 08	0·70341	+5·67	2·16	4·15	0·703574	0·703408	0·703271
Pargasite	0·91	105·8	0·025	0·703273 ± 11	0·70324	+2·87	—	—			
Plagioclase	—	—	—	—	—	+10·09	—	—			
02 OA90b											
Plagioclase	0·04	238·5	<0·001	0·703868 ± 11	0·70387	+4·98	—	—			
Green hornblende	0·10	23·8	0·012	0·704288 ± 15	0·70427	+2·39	—	—			

Table 5: continued

Sample	Rb (ppm)	Sr (ppm)	$^{87}Rb/^{86}Sr$	$^{87}Sr/^{86}Sr$	$(^{87}Sr/^{86}Sr)_i$[1]	$\delta^{18}O$ (‰)	LOI (%)[2]	W/R[3]	$(^{87}Sr/^{86}Sr)L1$[4]	$(^{87}Sr/^{86}Sr)L2$[5]	$(^{87}Sr/^{86}Sr)R$[6]
02 OA37b											
Plagioclase	0·23	312·1	0·002	0·704204 ± 15	0·70420	—	—	—			
Pargasite	0·31	41·6	0·021	0·703505 ± 15	0·70348	+3·94	—	—			
94 OAMa2											
Whole rock	0·016	175·0	0·0003	0·703219 ± 15	0·70322	+4·95	0·33	3·1	0·703264	0·703177	0·703158
Plagioclase	0·014	136·3	0·0003	0·703219 ± 11	0·70322	+4·79	—	—			
Clinopyroxene	—	—	—	0·703236 ± 13	0·70324	—	—	—			

[1]Initial $^{87}Sr/^{86}Sr$ ratio calculated at 95 Ma (Hacker, 1994).
[2]LOI is loss on ignition (in %).
[3]Water–rock ratio calculated assuming a closed system. The effective W/R ratio can be expressed by the following equation:

$$W/R \text{ effective} = [(^{87}Sr/^{86}Sr^{rock})_{final} - (^{87}Sr/^{86}Sr^{rock})_{initial}]/[(^{87}Sr/^{86}Sr^{seawater})_{initial} - (^{87}Sr/^{86}Sr^{rock})_{final}] \times (C^{rock}_{initial}/C^{seawater}_{initial})$$

where $(^{87}Sr/^{86}Sr^{rock})_{final}$ is the final measured Sr isotopic ratio in the sample, $(^{87}Sr/^{86}Sr^{rock})_{initial}$, corresponding to the initial mantle value, is taken as 0·70295 (Lanphere *et al.*, 1981), $(^{87}Sr/^{86}Sr^{seawater})_{initial}$ is the Cretaceous seawater Sr isotopic composition [$^{87}Sr/^{86}Sr \sim 0{\cdot}7073$ at 90 Ma after Burke *et al.* (1982)], $C^{seawater}_{initial}$ is the Sr content of 'normal' seawater and is taken as 8 ppm (de Villiers, 1999). For the $C^{rock}_{initial}$, it is assumed that the present Sr concentration measured is the same as the initial concentration.
[4]Sr isotopic ratios measured for liquid L1 extracted after the first step of the leaching experiment (6N HCl for 8 min at 70°C).
[5]Sr isotopic ratios measured for liquid L2 extracted after the second step of the leaching experiment (2·5N HCl for 30 min at 70°C).
[6]Sr isotopic ratios measured for residue obtained after a total acid digestion achieved after the extraction of L1 and L2 leachates.

Part of the same sample from the contact between the dyke and the gabbro yields a slightly lower Sr isotopic composition (0·70464) intermediate between the surrounding gabbro and the epidote dyke. It also has an intermediate Sr content (425 ppm). Acid leaching experiments performed on the whole rock of the dyke yield Sr isotopic compositions of 0·70521 and 0·70512, for the two liquids extracted. Similar experiments for the sample located at the contact with the gabbro yield $^{87}Sr/^{86}Sr$ ratios of 0·70494 and 0·70467, for L1 and L2 liquids. The Sr isotopic composition of the residue extracted after leaching remains high (0·70459) and very close to the epidosite $^{87}Sr/^{86}Sr$ ratio determined by Kawahata *et al.* (2001). In this sample, the primary minerals have been totally replaced by epidote and secondary plagioclase or quartz. Thus, the Sr isotopic compositions measured for this WR sample and its constituent minerals reflect the composition of the fluid filling this dyke.

Mineral chemistry

Plagioclase

Compared with the host gabbros, the dykes show a much larger dispersion in their plagioclase compositions (Fig. 8a and b, Table 4), characterized by more calcic plagioclase than the enclosing gabbros. This tendency is most extreme in the comb-textured dykes in which the plagioclase is almost pure anorthite. The zoning is generally normal, recording a crystal fractionation process. However, gabbro 94 MA2 exhibits inverse zoning; this tendency is also observed in plagioclases from dykes 01 OA19a and 01 OA15f. The higher calcium content of the plagioclase as well as the inverse zoning is consistent with an increase of water pressure during its crystallization (Turner & Verhoogen, 1960; Carmichael *et al.*, 1974; Koepke *et al.*, 2003). The particularly high An content in the comb-textured gabbro dykes 01 OA15f may also result from crystallization in a supercooled magma; this is consistent with the comb texture, indicative of fast-growing crystals. The lack of brown hornblende suggests that crystallization occurred above the temperature of hornblende stability.

Amphibole

The amphiboles analysed in the dykes (Fig. 8c and Table 4) show a regular trend in a $(Na + K)_A$ vs Al^{IV} diagram from titanium-rich (Ti > 0·15) pargasitic hornblende (brown amphibole) and tschermakite (brown–green amphibole), to low-titanium (Ti < 0·15) magnesio-hornblende (green amphibole), and actinolite (pale green amphibole). The pargasitic hornblende develops as poikilitic oikocrysts in the dykes 01 OA19a and d, and in the diffuse patch 01 OA41d2 at temperatures above 800°C, during the final stage of crystallization (see below). The tschermakite composition corresponds to the internal alteration of clinopyroxene in gabbro 94 Ma2, occurs in the comb-textured dyke 01 OA15f, and is the primary amphibole in the dioritic dyke 02 OA37b. The magnesio-hornblende develops at the edges of the pargasites or of clinopyroxenes at temperatures around 800°C, and is the primary phase in the dioritic dyke 02 OA90b and in the green vein 02 OA43a. Finally actinolite occurs as a replacement of green hornblende in dykes, or in the kelyphitic rim surrounding olivine in gabbro 94 Ma2. Such a large composition range at the scale of a thin section has been reported in amphiboles from amphibolite-facies oceanic gabbros (Stakes, 1991; Stakes & Taylor, 1992; Gillis *et al.*, 1993), as well as in the Oman ophiolite gabbros (Manning *et al.*, 2000). This variability has been explained by rapid reaction rates preventing homogenization (Manning *et al.*, 2000).

Thermometry

Plagioclase–amphibole thermometry could be applied when the two minerals exhibited good contacts, such as in the laminated gabbro of the middle sequence (01 OA41d2) and in the intrusive dykes. The temperatures of plagioclase–amphibole equilibration (Table 2) have been calculated using the geothermometer 'B' of Holland & Blundy (1994), Edenite + Albite = Richterite + Anorthite valid between 500°C and 900°C with an uncertainty of ±40°C. Amphibole formulae are based on 23 oxygen, and their nomenclature is based on alkali cations in the A site vs Al^{IV} according to Leake (1997). Pressure was assumed to be 1 kbar. Forty-five plagioclase–amphibole pairs meet the compositional criteria imposed by Holland & Blundy's dataset ($0·9 > X_{an} > 0·1$ and $Al^{IV} > 0·3$). Electron microprobe measurements were constrained to contiguous plagioclase and amphibole separated by sharp grain boundaries, assuming equilibrium of the two phases. When the mineral phases exhibit normal zoning, temperatures between plagioclase and amphibole cores, and between mineral rims, were calculated assuming that the temperatures deduced from the mineral core chemistry provide a proxy for the highest temperature of equilibration. These data are identified in the T°C vs Al^{IV} diagram (Fig. 8d). Table 4 presents selected major element amphibole analyses, the An content of the plagioclase adjacent to each amphibole grain, and the temperature calculated for the pair.

The temperatures calculated (Fig. 8d) span the entire range of temperatures at which amphibole and plagioclase coexist in equilibrium (i.e. amphibolite-facies parageneses). This temperature interval is bracketed by orthopyroxene-bearing facies or amphibole-free facies (i.e. gabbro 94 MA2) and epidote–actinolite facies devoid of homogeneous plagioclase (i.e. epidosite dyke 01 OA36b and green vein 02 OA43a). The range of the

calculated temperatures, between >900°C and 750°C, corresponds to the changing composition of amphiboles from pargasite to magnesio-hornblende at the scale of a thin section or even at that of an individual crystal, as shown by their correlation with Al^{IV}; such variability records rapid cooling in hydrous conditions. The highest temperatures are recorded by pargasite from the anatectic gabbro 01 OA41d2, in the gabbro dyke 01 OA19d and in the dioritic dyke 02 OA90b. They were calculated from minerals devoid of lower-grade alteration and are thus considered as representing the equilibrium temperature of the coexisting minerals. Lower temperatures correspond to mineral phases evolving at falling temperature and are only indicative of the cooling history. Including the 40°C uncertainty, seven pairs provide temperatures higher than 900°C, the limit of validity of the Holland & Blundy thermometer. However, we maintain these temperatures as indicative of the highest values of our dataset. These values are included in the average equilibrium temperature summarized in Table 2.

DISCUSSION

Distribution of hydrothermal alteration

Two distinct petrological events are recorded in the gabbro section of the Samail ophiolite and are documented in the present contribution: (1) the whole gabbro section is affected by a penetrative alteration; (2) the gabbro section is crosscut by various types of dykes and veins including hydrous minerals.

Penetrative alteration

The penetrative alteration developed in the gabbros at grain boundaries and locally invading the minerals is ubiquitous in the gabbro section. This penetrative alteration has been described as very high temperature (VHT), high temperature (HT), and low temperature (LT), based on alteration parageneses. The orthopyroxene coronas in the layered gabbro sample and the incipient appearance of brown pargasitic amphibole mark a lower thermal limit of the VHT alteration. By reference to the experimental work of Koepke *et al.* (2003), the temperature of equilibration for these reactions is estimated to be between 900 and 1000°C.

The preservation of the vertical distribution of VHT–HT facies (Figs 4 and 5), also pointed out by Manning *et al.* (2000), indicates that the hydrothermal alteration pattern fits the distribution of isotherms with depth at a fast-spreading ridge (i.e. Phipps Morgan & Chen, 1993; Dunn *et al.*, 2000; Fig. 2). Equilibrium temperatures for VHT parageneses as high as 900–1000°C suggest that VHT–HT hydrothermal alteration took place in a very restricted time interval at the limit of the cooling magma chamber. It is proposed that the penetrative alteration affecting the entire gabbro section is related to a pervasive network of microcracks, which act as a recharge system down to the Moho (Nicolas *et al.*, 2003).

Dykes and veins

The dykes are extremely varied, e.g. pegmatitic gabbros with comb-texture, microgabbros and amphibolitized dolerites, dioritic dykes, alignments of poikilitic hornblende, and finally diffuse hornblende-bearing patches. High-T gabbro and diorite dykes, and low-T green amphibole–epidote veins are connected.

In the dykes, textural evidence attests to suprasolidus conditions at least for the development of the pargasitic amphibole. Integrating the hornblende–plagioclase equilibration temperatures calculated for the studied samples, these temperatures are bracketed between 950°C and 875°C.

In the following discussion, we shall consider separately the microgabbro and dolerite dykes. The latter represent basaltic melt intrusions associated, upsection, with the diabase sheeted dykes and, downsection, possibly with the mafic dykes that are ubiquitous in the mantle section (Nicolas *et al.*, 2000). Whatever their origin, the development of pargasitic amphibole during their late stage of crystallization creates a link with the gabbroic dykes and suggests a crystallization process evolving from dry conditions to more hydrous conditions.

The other gabbroic dykes, comb-textured gabbros and hornblende-bearing dioritic dykes result from the filling of cracks by a fluid, either a melt or a silica-rich hydrous fluid. These intrusive dykes, which develop reaction margins at their contact with the host gabbro, grade vertically into lower-temperature green amphibole veins, or alignments of poikilitic hornblende in the layered gabbro matrix, or development of pargasitic hornblende in anatectic gabbros (sample 01 OA41d2). In gabbros crystallizing in the magma chamber, the development of orthopyroxene and pargasite oikocrysts enclosing the primary minerals suggests a thermal evolution from the gabbro solidus to amphibolite-facies conditions. For these reasons, it is suggested that the gabbroic dykes resulted from the injection of a hydrous melt in the still hot gabbros drifting away from the magma chamber, as discussed below.

Origin of fluids responsible for VHT–HT hydrothermal alteration

The $^{87}Sr/^{86}Sr$ initial ratios and $\delta^{18}O$ of whole rocks and pure mineral fractions are plotted in Fig. 9 against the distance above the Moho Transition Zone (MTZ). The initial Sr isotopic composition of the whole rocks, apart from the epidosite dykes, ranges from 0·70322 to

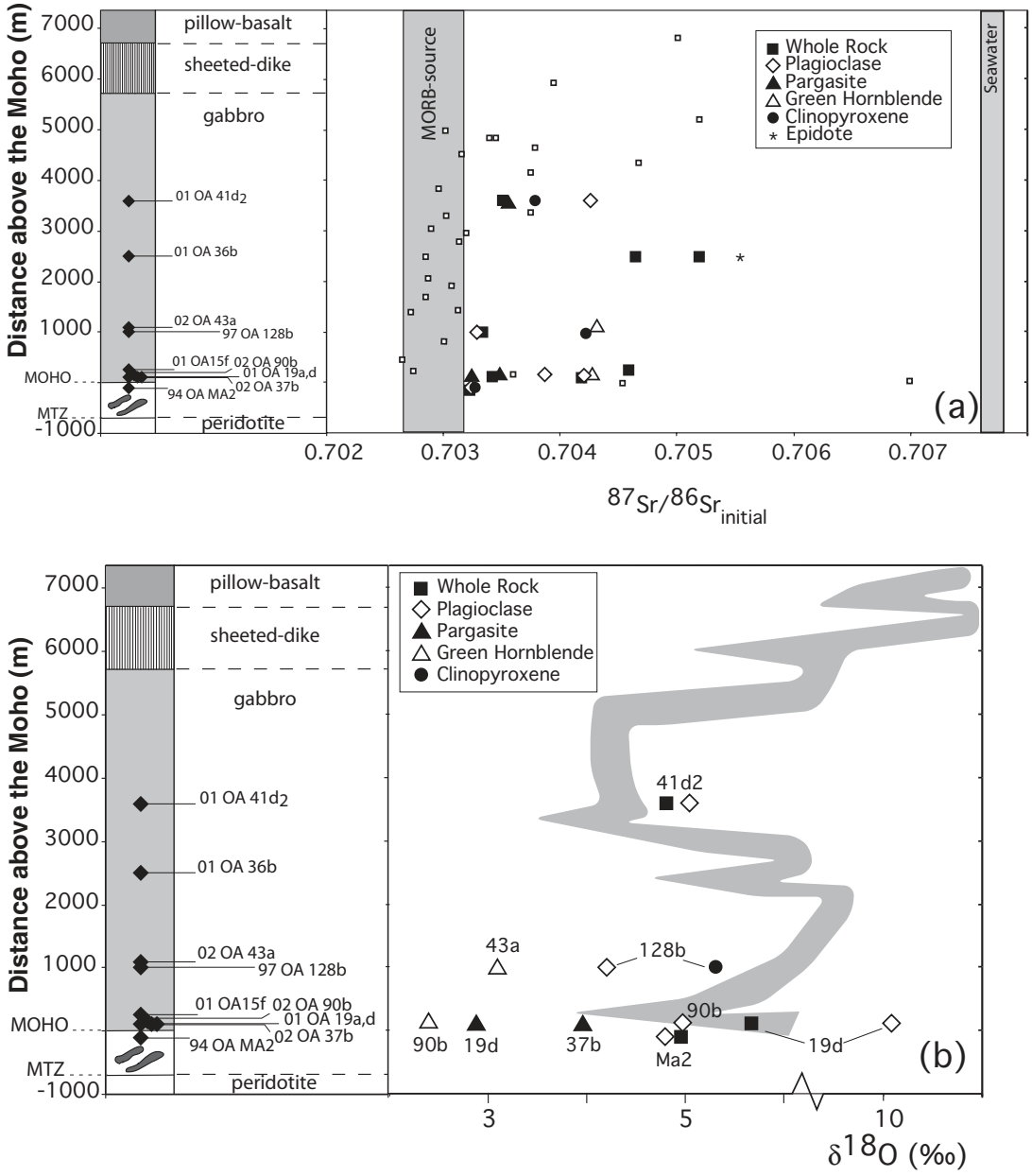

Fig. 9. (a) Variation of initial $^{87}Sr/^{86}Sr$ isotopic composition as a function of the location of the studied samples in a schematic log of the crustal section of the Oman ophiolite. The field for MORB is from Hart *et al.* (1974) and that for seawater is from Burke *et al.* (1982). Small open squares are data from Kawahata *et al.* (2001). (b) Variation of $\delta^{18}O$ (‰) as a function of the location of the studied samples in a schematic log of the crustal section of the Oman ophiolite. Shaded curve corresponds to the data of Gregory & Taylor (1981).

0·70458. All the studied samples (including whole rocks and minerals) have initial $^{87}Sr/^{86}Sr$ ratios falling outside the field of fresh MORB, which commonly have Sr ratios between 0·7023 and 0·7029 with an average of 0·70265 (i.e. Hart *et al.*, 1974). The lowest initial Sr isotopic composition (0·70322) from the massive gabbro 94 MA2 is slightly but significantly higher than average Oman primary magmatic signatures (i.e. 0·70296; McCulloch *et al.*, 1981). Similarly the $\delta^{18}O$ values of most whole rocks and minerals measured (Table 5) depart from typical MORB-source mantle values (Javoy, 1980; Gregory & Taylor, 1981; Kyser, 1986). These differences indicate that the primary mantle signatures in the Oman ophiolite have been modified by interaction with a fluid. Possible origins for this fluid are mantle components, dehydration of subducted lithosphere, or seawater circulation. Strontium and oxygen isotopes are useful tracers for fluid–crust interaction, as $\delta^{18}O$ and $^{87}Sr/^{86}Sr$ ratios from fluids originating from seawater, the mantle or subducted lithosphere

are significantly different. Moreover, the $\delta^{18}O$ value is dependent on temperature and mineral fractionation, and thus yields complementary constraints to Sr isotopes.

Mantle origin

One model to explain the occurrence of fluids interacting with the oceanic crust at very high temperatures is to derive them from the mantle. The contribution of mantle-derived hydrous fluids, linked to percolation processes or to their concentration in the final stages of gabbro crystallization has been invoked in numerous case studies (i.e. Witt & Seck, 1989; Fabriès *et al.*, 1989; Dupuy *et al.*, 1991; Agrinier *et al.*, 1993). O and Sr isotopic data for whole rocks and mineral separates yield scattered values that are unambiguously different from MORB mantle-source values (Fig. 9a and b). With the exception of late LT altered samples, the WR data have a mean $^{87}Sr/^{86}Sr$ ratio of 0·70337 and a standard deviation of 0·00012. These surprisingly high values in mantle-derived rocks could be taken as evidence for survival of mantle isotopic heterogeneities during crystallization of the ophiolite (e.g. Lanphere, 1981; McCulloch *et al.*, 1981). However, the $^{18}O/^{16}O$ isotope ratios in the Oman gabbroic sequence are also displaced from primary magmatic values. No gabbro, in the present study, has plagioclase or amphibole with typical mantle $\delta^{18}O$ values. Thus, the Sr and O isotope data rule out the possibility of mantle-derived fluids as a possible source for the VHT–HT hydrous alteration event recorded in the massive gabbros and gabbroic dykes and veins (Fig. 10a and b).

Subducted lithosphere origin

Dehydration of subducted oceanic crust in subduction zones can generate hydrous fluids. Such fluids could percolate through the overlying lithosphere and contaminate it, thus generating modified isotopic signatures and trace element contents. Such an explanation, however, disagrees with the geochemical characteristics of most of the studied samples. Fluids derived from the dehydration of subducted slabs (fresh or altered MORB, or OIB protoliths) should be strongly enriched in K, Rb and Ba (e.g. Becker *et al.*, 2000) whereas in Oman the Rb contents measured in the gabbros and gabbroic dykes and veins are strongly depleted. Moreover, the isotopic composition of slab-derived fluids is buffered by the MORB-like oceanic crustal protolith for Nd and Pb but not for Sr and O (Staudigel *et al.*, 1995). As a result of relatively minor fractionation of oxygen at high temperature, the oxygen isotope composition of the fluids expelled during dehydration of the subducted slab should be high and essentially controlled by the oxygen composition of the upper section of the crust altered at low temperature (with an average of 10‰ and perhaps as high as 19‰) (Staudigel *et al.*, 1995). The Sr isotopic composition should be also high (average 0·7046), as the fluids released by the dehydration of subducted oceanic crust are associated either with seawater or with radiogenic Sr phases (i.e. smectites). The Sr and O isotopic compositions of the studied samples do not fit with these signatures and so preclude a subducted lithosphere origin for the fluids involved in the VHT–HT alteration event.

Seawater-derived fluids

All the analysed samples (minerals and WR) have $^{87}Sr/^{86}Sr_{(T)}$ outside the domain of primary MORB magmas and variable Sr contents. Individual minerals have Sr contents reflecting their different mineral/liquid partition coefficients. Minerals characterized by a very high affinity for Sr such as plagioclase (i.e. Sr mineral/liquid partition coefficients ? 1) have very high Sr contents. Therefore, the high abundance of plagioclase in the samples analysed is responsible for the high Sr content of the studied whole rocks. The Sr content of all the whole rocks is relatively homogeneous (Table 5) without clear distinction between country-rock gabbros and dykes and veins, and ranges from 110 to 200 ppm except for the epidosite (>700 ppm). Reported on a $^{87}Sr/^{86}Sr$ vs 1/Sr diagram (Fig. 10a), most whole rocks and plagioclases analysed are characterized by a 1/Sr ratio lower than 0·01 and plot in the left part of this diagram. Compared with N-MORB, the studied massive and anatectic gabbros and their constituent plagioclases have similar to slightly higher Sr contents but substantially higher $^{87}Sr/^{86}Sr$ ratios (Fig. 10a). Considering Cretaceous seawater as a possible high $^{87}Sr/^{86}Sr$ mixing component [$^{87}Sr/^{86}Sr \sim 0{\cdot}7073$ at 90 Ma after Burke *et al.* (1982)] responsible for the observed geochemical modifications, exchanges cannot have occurred in a closed system, as seawater has too low a Sr content (i.e. 8 ppm; de Villiers, 1999). An open-system process allowing penetration of larger quantities of seawater can efficiently modify the Sr isotopic ratio of the rocks. Alternately, the fluids could also be seawater that was modified through exchange with the surrounding rocks during its transit through the oceanic crustal section. This modified seawater would be more enriched in Sr with a $^{87}Sr/^{86}Sr$ ratio intermediate between unmodified seawater and MORB.

Minerals devoid of late LT alteration imprints (pargasite, green hornblende and pyroxene) and characterized by very low Sr contents plot on the right of the diagram, close to, or on the mixing line between seawater and MORB (Fig. 10a). The difference between these minerals and the other samples (WR and plagioclases) is mainly due to the Sr fractionation coefficients of these different minerals and to the large quantity of plagioclase in the studied rocks. The process responsible for the

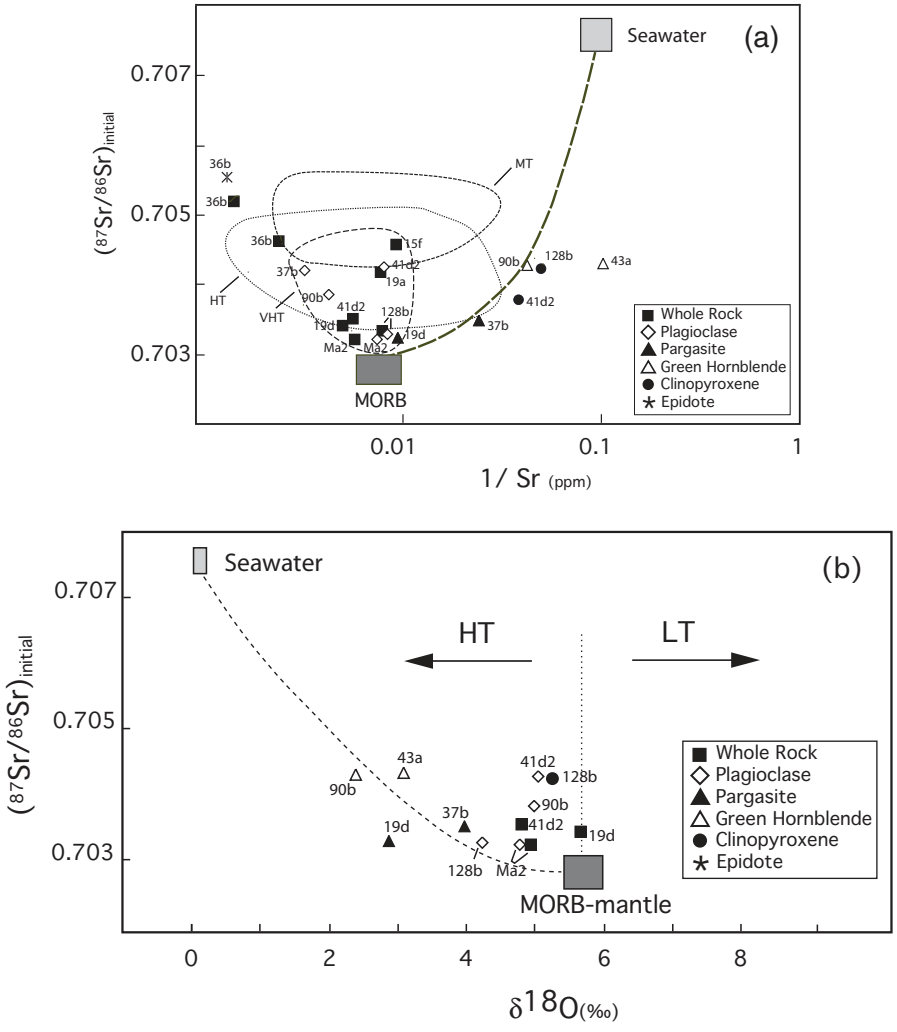

Fig. 10. (a) Initial $^{87}Sr/^{86}Sr$ isotopic ratios plotted against 1/Sr for whole rocks and mineral separates from the gabbro section of the Oman ophiolite. Fields shown are from Kawahata *et al.* (2001) and correspond to: MT—basalt, sheeted dyke diabase altered at medium temperature (prehnite–actinolite facies, sequence 3); HT—diabase, plagiogranite, metagabbro and epidosite formed at high temperature (greenschist facies, sequence 4); VHT—gabbro altered at very high temperature (amphibolite facies, sequence 5). The dashed line is a binary mixing line between MORB (Lanphere *et al.*, 1981) and Cretaceous seawater (Burke *et al.*, 1982). (b) Initial $^{87}Sr/^{86}Sr$ isotopic composition plotted against $\delta^{18}O$ value for whole rocks and minerals from the Oman ophiolite. Cretaceous seawater and MORB end-members as in (a). Dashed line represents mixing curve between MORB and seawater at high temperature (HT). Low-temperature (LT) exchanges between these two components would be responsible for an increase of the $\delta^{18}O$ primary MORB value.

modification of the Sr isotopic composition from MORB-source value is, however, explained by the same phenomenon. As all these minerals display initial $^{87}Sr/^{86}Sr$ ratios distinct from the MORB source and because they equilibrated at VHT or HT temperatures, this supports an early intervention of seawater during crystallization of these minerals. Most of these samples, with the exception of the epidosite dyke, overlap the domains defined by Kawahata *et al.* (2001) for the Wadi Fizh gabbros altered at VHT and HT conditions in the amphibolite facies (labelled 'VHT' and 'HT' in Fig. 9a).

Three samples (two epidosite dykes and an one epidote fraction) have very high Sr contents and the highest Sr isotopic compositions of the present dataset. The two whole-rock samples overlap the field of the Wadi Fizh samples altered at high temperature, during greenschist-facies metamorphism (Kawahata *et al.*, 2001). This type of alteration is common at the ridge axis and formed through intensive exchange with seawater-derived fluids.

Figure 10b indicates that all the Sr–O isotope data are distinct from MORB compositions and suggests that the fluids reacting with the magmas could be derived from seawater. In addition, the $\delta^{18}O$ values show that isotopic exchange occurred under VHT or HT conditions. The fluids could have the composition of seawater or they could have the composition of seawater modified through

exchange with the surrounding rocks during its penetration into the crustal section. In an environment in which fluid–rock interaction occurs at variable temperatures, the $\delta^{18}O$ is greatly influenced by the temperature at which the exchange took place and by the water/rock ratio. It is evident from Figs 9b and 10b that none of the studied gabbros have plagioclase and amphibole with MORB-like $\delta^{18}O$ and $^{87}Sr/^{86}Sr$ values. The separate minerals display a broad range of $\delta^{18}O$ values and most exhibit extreme ^{18}O depletion (Table 5). Hydrothermal exchange kinetics are similar in amphibole and pyroxene and these two minerals are more resistant to oxygen exchange during water–rock interaction than coexisting plagioclase (Gregory *et al.*, 1989). The most probable explanation of the low $\delta^{18}O$ values measured in both amphiboles and pyroxenes is that they crystallized at high temperature in the presence of a relatively low ^{18}O seawater-derived hydrothermal fluid [$\delta^{18}O$ from $-0{\cdot}1$ to $-0{\cdot}7$ after Gregory & Taylor (1981)]. The anomalously high $\delta^{18}O$ value ($+10{\cdot}09$) measured for the plagioclase of the micro-gabbroic dyke (01 OA19d) can be interpreted as resulting from a superimposed overprint caused by a late-stage penetration of fluids at lower temperature. In this sample, the occurrence of such different $^{18}O/^{16}O$ ratios between coexisting plagioclase and amphibole is not consistent with equilibrium fractionation between these two minerals at any possible temperature. This observation suggests that parts of the ophiolite sequence have undergone a high-temperature hydrothermal event prior to the later low-temperature event that produced the strong ^{18}O increase in coexisting plagioclase. The depletion of the $\delta^{18}O$ values results from high-temperature hydrothermal alteration (Gregory & Taylor, 1981; Stakes & Taylor, 1992). The oxygen isotopic data support the contention that most studied samples have been affected by a VHT–HT hydrothermal alteration by fluids derived from seawater. Some of the analysed samples, presenting petrological evidence of crystallization of LT secondary minerals, have been overprinted by the late low-temperature alteration, thus swamping the earlier high-temperature alteration effects.

Determination of water/rock ratio

To better evaluate the exchange between seawater and the gabbroic rocks, water/rock ratios (W/R) have been estimated for the whole rocks analysed during the course of this study. The different models used to constrain this ratio mainly differ by the calculation of the effective ratio or by the estimated weight ratio and by considering open or closed systems for water circulation (Albarède *et al.*, 1981; McCulloch *et al.*, 1981). The W/R ratios reported in Table 5 have been calculated assuming a closed system. Using this formulation, these values are minima because the calculation always uses pristine fluid for the initial fluid, thus maximizing the value in the denominator. If the fluid was shifted to lower ^{87}Sr concentrations by exchange with the rock on the downward path, the inferred values would be much higher (Davis *et al.*, 2003).

The calculated W/R ratios for the samples from this study range from 3·1 to 21·9 (Table 5). Two main groups of samples can be recognized on the basis of their water/rock ratios. The lowest ratios, ranging from 3·1 to 4·7, have been determined for massive gabbros or anatectic gabbros but also for dykes and veins devoid of late LT alteration. Similar ratios have been previously calculated, for example, for the discharged hydrothermal solutions at the 13°N and 21°N East Pacific Rise (Di Donato *et al.*, 1990; Fouquet *et al.*, 1991). The gabbros from the Ibra section in the Oman ophiolite gave effective W/R ratios of 0·5, 3·3 and 4·2 (McCulloch *et al.*, 1981) in good agreement with the values obtained in this study. The least altered gabbro of the Ibra section yields a W/R ratio of 0·5, in good agreement with the exceptionally freshness of this rock characterized by typical mantle oxygen values for its minerals (McCulloch *et al.*, 1981). Samples characterized by water/rock effective ratios in the range of 3–5 can be related to penetrative alteration via the hydrothermal system. Lecuyer & Reynard (1996) have demonstrated in oceanic gabbros from the Hess Deep, altered in similar HT conditions, that W/R mass ratios in the range of 0·2–1 are sufficient to account for the modified stable isotope signature of the gabbros. Higher water/rock values ($W/R > 5$) have been calculated for samples affected by superimposed late hydrothermal alteration and for the epidosite samples (Table 5). They probably acquired their isotopic characteristics through interaction with a larger volume of seawater during greenschist-facies metamorphism. Similar or higher W/R values have been published in previous studies (i.e. McCulloch *et al.*, 1981; Kawahata *et al.*, 2001). They correspond either to samples from the upper-crustal sequence (i.e. basalt, sheeted dyke or plagiogranite) or to gabbros from the crustal section located in a particular environment such as, for example, the Wadi Fizh section that is located close to a segment boundary along the palaeo-spreading axis (Nicolas *et al.*, 2000).

Mechanism for seawater interaction with magma

Nicolas *et al.* (2003) have proposed that variable amounts of seawater can circulate, at high temperature, throughout the crustal section down to the walls of the magma chamber, via a network of parallel microcracks a fraction of a millimetre wide. Such microcracks and their relationship with the VHT–HT hydrous alteration in the surrounding gabbros have been described in detail by Nicolas *et al.* Via this network of microcracks, large amounts of seawater can have reacted with the magma

and induced variable changes of its Sr and O isotopic composition. This regular network of parallel microcracks could constitute the recharge system and the hydrated gabbroic dykes the discharge system. Physical parameters and the geophysical models of Nicolas *et al.* (2003) are in agreement with this scenario. Such a penetration of seawater-derived hydrothermal fluids through the lower crust along grain boundaries and a microscopic fracture network at temperatures >750°C is consistent with recent thermodynamic models (McCollom & Shock, 1998).

Seawater-altered and high-temperature recrystallized diabases (protodykes) from the overlying sheeted dyke complex stoped into the melt lenses could represent an indirect way for seawater to enter the system, as they can remelt during their subsidence through the magma chamber. A simple mass balance calculation suggests that this indirect contamination is not significant. Assessments of the amount of recycled crust, ~1% in volume by Nicolas *et al.* (2000) based on the protodyke remnants in the gabbro section, or 20% by Coogan *et al.* (2003) based on chlorine content in EPR basalts, lead to a seawater/rock ratio of the order of 10^{-4} to 10^{-3}.

Thus, following Nicolas *et al.* (2003), we propose that seawater has been introduced along microcracks down to the walls of the magma chamber, and has diffused along grain boundaries in the way described by Manning *et al.* (2000), progressively invading the host gabbro. Gabbroic dykes result from the injection of hydrous melt into the host gabbros at falling temperatures, as they drift away from the magma chamber. This water-saturated melt could result from the extensive hydration of the crystallizing gabbros near the walls of the magma chamber, when seawater penetrates through this wall (Fig. 1).

Similar plumbing systems driving seawater down to the limit of the magma chamber and back to the surface have been already proposed in other environments such as the Mid-Atlantic Ridge (Kelley & Delaney, 1987; Coogan *et al.*, 2001), the East Pacific Rise at Hess Deep (Gillis, 1995; Manning *et al.*, 1996*a*, 1996*b*), the Tonga forearc (Banerjee & Gillis, 2001), and the Troodos ophiolite (Gillis & Roberts, 1999). The melting curve of wet basalt has a negative slope, but is close to the dry solidus at low pressure in the lower gabbros and the first melts are plagiogranitic (Spulber & Rutherford, 1983). Such plagiogranites are ubiquitous in the highest gabbros and in the root zone of sheeted dykes in Oman (Rothery, 1983; Juteau *et al.*, 1988; Nicolas & Boudier, 1991), in many other ophiolites and in the oceanic crust, where they have been interpreted as resulting either from wet anatexis of hot gabbros or from the final product of crystallization of a basaltic melt (Spulber & Rutherford, 1983). Plagiogranites are rare in the lower gabbros, exceptionally associated with hydrous gabbro segregations inside the layered gabbros. Their constitutive minerals are also remarkably absent along the VHT microcracks, although these gabbros were above the wet solidus. A possible explanation has been proposed by McCollom & Shock (1998), who wrote that, at high temperature, 'aqueous fluids may leave very little conspicuous petrological evidence for their presence', the reason being that the high-T conditions would be closer to batch melting. Obviously, more detailed studies on this specific problem are needed. We conclude that the large degree of hydrous melting locally required at the walls of the magma chamber to account for the generation of a gabbroic hydrous melt may have erased the traces of the incipient plagiogranitic melt.

CONCLUSIONS

Fostered by the recent discovery of high-temperature seawater contamination in some gabbros of the Oman ophiolite (Manning *et al.*, 2000), we have conducted a study on 500 gabbro specimens from selected areas of the entire Samail ophiolite belt and on the hydrous gabbroic dykes that cross-cut them. The highest-temperature reactions (VHT) recorded in olivine and clinopyroxene in gabbros as orthopyroxene and pargasite coronas reach 975°C. They are followed at lower HT conditions with replacement of olivine by an assemblage of tremolite, magnetite and plagioclase surrounded by chlorite, and by pargasite development in clinopyroxene, followed finally by the LT lizardite–olivine and saussurite–plagioclase greenschist-facies alteration. With a few exceptions, the VHT alteration tends to be restricted to the lower gabbros and to the vicinity of the Moho, and the HT alteration to the middle and upper gabbros. The preservation of the vertical distribution of VHT–HT facies indicates that progressive cooling during off-axis spreading did not obliterate this distribution, and consequently that the VHT–HT hydrothermal alteration took place in a very restricted time interval at the limit of the cooling magma chamber. In the deep and hot gabbros, the main water channels may be sub-millimetre-sized microcracks with a dominantly vertical attitude, the origin and dynamics of which have been investigated in a previous paper (Nicolas *et al.*, 2003).

Beyond these high-temperature alteration zones massively induced in the gabbros, seawater may be responsible for the generation of clinopyroxene–pargasite gabbro dykes that cross-cut all gabbros and that are, upsection, clearly connected to the LT hydrothermal vein system. Petrostructural evidence suggests that these dykes were generated by hydration of the crystallizing gabbros near the internal wall of the LVZ–magma chamber. The resultant melts were subsequently intruded at various levels in the cooling lower and middle gabbros. Petrological observations of nearly all the gabbros analysed in the present study, located from the root zone of

the sheeted dyke complex down to the Moho, emphasize the imprint of VHT–HT hydrous alteration. The VHT hydrothermal event is characterized by temperatures of equilibration around 900–1000°C. The temperatures at which the HT hydrous event occurred are estimated to be in the range 550–900°C.

Strontium and oxygen isotope compositions measured on whole rocks and separated minerals significantly depart from primary MORB values. The Sr and O isotope data obtained for pargasite, green hornblende and clinopyroxene record the participation of seawater at the temperature of crystallization of the minerals. Plagioclases and whole rocks define a trend toward a component characterized by a high radiogenic $^{87}Sr/^{86}Sr$ value and a higher Sr content than normal seawater. Seawater is clearly identified as the fluid responsible for the modification of the Sr and O signatures for both massive gabbros and dykes and veins. Nevertheless, the high Sr content of the extraneous component requires either open-system exchange allowing penetration of a greater quantity of seawater, or penetration of seawater modified by interaction with the oceanic crust during its travel path through the crustal section. The water/rock ratio calculated on the basis of the Sr isotopes is between three and five for the enclosing gabbros and for the least LT altered dykes. The VHT–HT hydrothermal event affecting these samples is related to penetrative alteration via the recharge and discharge hydrothermal system. The water/rock ratio is $\sim$10 for dykes exhibiting evidence of a LT hydrothermal alteration overprint, and reaches 22 for the epidosite dyke. The depletion in $\delta^{18}O$ characterizes all the studied samples with the single exception of the micro-gabbroic dyke plagioclase. This agrees with the conclusions based on Sr isotopes suggesting that these samples have undergone exchange with seawater-derived fluids during a VHT–HT alteration hydrothermal event.

ACKNOWLEDGEMENTS

This work has benefited from financial support by the Centre National de la Recherche Scientifique (INSU Intérieur-Terre and DYETI programmes), and, in Oman, from the willingness of the Directorate of Minerals, Ministry of Commerce and Industry, and the hospitability of the people. Technical help in the laboratory is also acknowledged, including C. Nevado for the thin sections, E. Ball for the illustrations, B. Galland for her assistance in the chemistry room and C. Bassoulet for help during thermal ionization mass spectrometric analyses of the Sr results from the leaching experiments. Constructive reviews from R. T. Gregory, C. Lecuyer, an anonymous reviewer, and particularly from M. Wilson, greatly helped to improve an earlier version of the manuscript.

REFERENCES

Agrinier, P., Mevel, C., Bosch, D. & Javoy, M. (1993). Metasomatic hydrous fluids in amphibole peridotites from Zabargad Island (Red Sea). *Earth and Planetary Science Letters* **120**, 187–205.

Albarède, F. A., Michard, A., Minster, J. F. & Michard, G. (1981). $^{87}Sr/^{86}Sr$ ratios in hydrothermal waters and deposits from the East Pacific Rise at 21°N. *Earth and Planetary Science Letters* **55**, 229–236.

Banerjee, N. R. & Gillis, K. M. (2001). Hydrothermal alteration in a modern subduction zone: the Tonga forearc crust. *Journal of Geophysical Research* **106**(B10), 21737–21750.

Becker, H., Jochum, K. P. & Carlson, R. W. (2000). Trace element fractionation during dehydration of eclogites from high-pressure terranes and the implications for element fluxes in subduction zones. *Chemical Geology* **163**, 65–99.

Benoit, M., Polve, M. & Ceulener, G. (1996). Trace element and isotopic characterization of mafic cumulates in a fossil mantle diapir (Oman ophiolite). *Chemical Geology* **134**, 199–214.

Bosch, D. (1991). Introduction d'eau de mer dans le diapir mantellique de Zabargad (Mer Rouge) d'après les isotopes du Sr et du Nd. *Comptes Rendus de l'Académie des Sciences* **313**, 49–56.

Boudier, F., Godard, M. & Ambruster, C. (2000). Significance of noritic gabbros in the gabbro section of the Oman ophiolite. *Marine Geophysical Research* **21**(3–4), 307–326.

Burke, W. H., Denison, R. E., Hetherington, R. B., Koepnick, R. B., Nelson, H. F. & Otto, H. F. (1982). Variation of seawater $^{87}Sr/^{86}Sr$ throughout Phanerozoic time. *Geology* **10**, 516–519.

Carmichael, I. S. E., Turner, F. J. & Verhoogen, J. (1974). *Igneous Petrology*. Berkeley, CA: University of California, Berkeley, 739 pp.

Chernosky, J. V., Berman, R. G. & Bryndzia, L. T. (1988). Stability, phase relations, and thermodynamic properties of chlorite and serpentine group minerals. In: Bayley, S. W. (ed.) *Hydrous Phyllosilicates. Mineralogical Society of America, Reviews in Mineralogy* **19**, 295–346.

Coogan, L. A., Wilson, R. N., Gillis, K. M. & MacLeod, C. J. (2001). Near-solidus evolution of oceanic gabbros: insights from amphibole geochemistry. *Geochimica et Cosmochimica Acta* **65,** 4339–4357.

Coogan, L. A., Mitchell, N. C. & O'Hara, M. J. (2003). Roof assimilation at fast spreading ridges: an investigation combining geophysical, geochemical, and field evidence. *Journal of Geophysical Research on line first*. http://www.agu.org/pubs/current/jb/, **108**(B1), 1171.

Davis, A. C., Bickle, M. J. & Teagle, D. A. H. (2003). Imbalance in the oceanic strontium budget. *Earth and Planetary Science Letters* **211**, 173–187.

Detrick, R. S., Buhl, P., Vera, E., Mutter, J., Orcutt, J., Madsen, J. & Trocher, T. (1987). Multi-channel seismic imaging of a crustal magma chamber along the East Pacific Rise. *Nature* **326**, 35–41.

De Villiers, S. (1999). Seawater strontium and Sr/Ca variability in the Atlantic and Pacific oceans. *Earth and Planetary Science Letters* **171**, 623–634.

Di Donato, G., Joron, J. L., Treuil, M. & Loubet, M. (1990). Geochemistry of zero-age N-MORB from hole 648B, ODP legs 106–109, M.A.R., 22°. In: Detrick, R. S., Honnorez, J., *et al.* (eds) *Proceedings of the Ocean Drilling Program, Scientific Results, 106/109*. College Station, TX: Ocean Drilling Program, pp. 57–65.

Dunn, R. A., Toomey, D. R. & Solomon, S. C. (2000). Three-dimensional seismic structure and physical properties of shallow mantle beneath the East Pacific Rise at 9°30′N. *Journal of Geophysical Research* **105**, 23537–23555.

Dupuy, C., Mevel, C., Bodinier, J. L. & Savoyant, L. (1991). Zabargad peridotite: evidence for multistage metasomatism during Red Sea rifting. *Geology* **19**, 722–725.

Fabriès, J., Bodinier, J. L., Dupuy, C., Lorand, J. P. & Benkerrou, C. (1989). Evidence for modal metasomatism in the orogenic spinel lherzolite body from Caussou (northeastern Pyrenees, France). *Journal of Petrology* **30**, 199–228.

Fouquet, Y., Von Stackelberg, S. U., Charlou, J. L., Donval, J. P., Foucher, J., Erzig, P., Muhe, R., Wiedicke, M., Soakai, S. & Whitechurch, H. (1991). Hydrothermal activity in the Lau back-arc basin: sulfides and water chemistry. *Geology* **19**, 303–306.

Gillis, K. M. (1995). Controls on hydrothermal alteration in a section of fast-spreading oceanic crust. *Earth and Planetary Science Letters* **134**, 473–489.

Gillis, K. M. & Roberts, M. (1999). Cracking at the magma–hydrothermal transition: evidence from the Troodos ophiolite. *Earth and Planetary Science Letters* **169**, 227–244.

Gillis, K. M., Mevel, C., *et al.* (eds) (1993). *Proceedings of the Ocean Drilling Program, Initial Reports, 147*. College Station, TX: Ocean Drilling Program.

Gregory, R. T. & Taylor, H. P. (1981). An oxygen isotope profile in a section of Cretaceous oceanic crust, Samail ophiolite, Oman: evidence for δ18O buffering of the oceans by deep (>5 km) seawater–hydrothermal circulation at mid-ocean ridges. *Journal of Geophysical Research* **86**(B4), 2737–2755.

Gregory, R. T., Criss, R. E. & Taylor, H. P. (1989). Oxygen isotope exchange kinetics of mineral pairs in closed and open systems: applications to problems of hydrothermal alteration of igneous rocks and Precambrian iron formations. *Chemical Geology* **75**, 1–42.

Hacker, B. R. (1994). Rapid emplacement of young oceanic lithosphere, argon geochronology of the Oman ophiolite. *Science* **265**, 1563–1569.

Hart, S. R., Erlank, A. J. & Kable, J. D. (1974). Sea floor basalt alteration: some chemical and Sr isotopic effects. *Contributions to Mineralogy and Petrology* **44**, 219–230.

Holland, T. & Blundy, J. (1994). Non-ideal interactions in calcic amphiboles and their bearing on amphibole–plagioclase thermometry. *Contributions to Mineralogy and Petrology* **116**, 433–447.

Ionov, D. A., Savoyant, L. & Dupuy, C. (1992). Application of the ICP-MS technique to trace element analysis of peridotites and their minerals. *Geostandards Newsletter* **16**, 311–315.

Javoy, M. (1980). $^{18}O/^{16}O$ and D/H ratios in high temperature peridotites. In: *Colloques Internationaux du CNRS* **272**, 279–287.

Juteau, T., Beurrier, M., Dahl, R. & Nehlig, P. (1988). Segmentation at a fossil spreading axis: the plutonic sequence of the Wadi Haymiliyah area (Haylayn Block, Sumail nappe, Oman). *Tectonophysics* **151**, 167–197.

Juteau, T., Manac'h, G., Moreau, C., Lecuyer, C. & Ramboz, C. (2000). The high temperature reaction zone of the Oman ophiolite: new field data, microthermometry of fluid inclusions, PIXE analyses and oxygen isotopic ratios. *Marine Geophysical Research* **21**, 351–385.

Kawahata, H., Nohara, M., Ishizuka, H., Hasebe, S. & Chiba, H. (2001). Sr isotope geochemistry and hydrothermal alteration of the Oman ophiolite. *Journal of Geophysical Research* **106**, 11083–11099.

Kelemen, P. B. & Aharonov, E. (1998). Periodic formation of magma fractures and generation of layered gabbros in the lower crust beneath oceanic spreading ridges. *Annual Geological Union Special Monograph* **106**, 267–289.

Kelemen, P. B., Koga, K. & Shimizu, N. (1997). Geochemistry of gabbro sills in the crust/mantle transition zone of the Oman ophiolite: implications for the origin of the oceanic lower crust. *Earth and Planetary Science Letters* **146**, 475–488.

Kelley, D. S. & Delaney, J. R. (1987). Two-phase separation and fracturing in mid-ocean ridge gabbros at temperatures greater than 700°C. *Earth and Planetary Science Letters* **83**, 53–66.

Koepke, J., Feig, S. T., Snow, J. & Freise, M. (2003). Petrogenesis of oceanic plagiogranites by partial melting of gabbros: an experimental study. *Contributions to Mineralogy and Petrology on line first*. http://www.springerlink.com/openurl.asp?genre=s00410-003-0511-9.

Kyser, T. K. (1986). Stable isotope variations in the mantle. In: Valley, J. W., Taylor, H. P. & O'Neil, J. R. (eds) *Stable Isotopes in High Temperature Geological Processes. Mineralogical Society of America, Reviews in Mineralogy* **16**, 141–164.

Lanphere, M. A. (1981). K–Ar ages of metamorphic rocks at the base of the Samail ophiolite, Oman. *Journal of Geophysical Research* **86**, 2777–2782.

Lanphere, M. A., Coleman, R. G. & Hopson, C. A. (1981). Sr isotopic tracer study of the Samail ophiolite, Oman. *Journal of Geophysical Research* **86**(B4), 2709–2720.

Leake, B. E. (1997). Nomenclature of amphiboles report of the subcommittee on amphiboles of the International Mineralogical Association commission on new minerals and mineral names. *European Journal of Mineralogy* **9**, 623–651.

Lecuyer, C. & Reynard, B. (1996). High-temperature alteration of oceanic gabbros by seawater (Hess Deep, Ocean Drilling Program Leg 147): evidence from oxygen isotopes and elemental fluxes. *Journal of Geophysical Research* **101**(B7), 15883–15897.

Liou, J. G., Kuniiyoshi, S. & Ito, K. (1974). Experimental study of the phase relations between greenschist and amphibolite in a basaltic system. *American Journal of Science* **274**, 613–632.

MacLeod, C. J. & Rothery, D. A. (1992). Ridge axial segmentation in the Oman ophiolite: evidence from along-strike variations in the sheeted dyke complex. *Geological Society of America, Special Papers* **60**, 39–63.

Manning, C. E., MacLeod, C. J. & Weston, P. E. (1996*a*). Fracture-controlled metamorphism of Hess Deep gabbros, site 984: constraints on the roots of mid-ocean ridge hydrothermal systems at fast-spreading centers. In: Gillis, M. C., Allan, K. M. & Meyer, P. S. (eds) *Proceedings of the Ocean Drilling Program, Scientific Results, 147*. College Station, TX: Ocean Drilling Program, pp. 189–211.

Manning, C. E., Weston, P. E. & Mahon, K. I. (1996*b*). Rapid high-temperature metamorphism of East Pacific Rise gabbros from Hess Deep. *Earth and Planetary Science Letters* **144**, 123–132.

Manning, C. E., MacLeod, C. J. & Weston, P. E. (2000). Lower-crustal cracking front at fast-spreading ridges: evidence from the East Pacific Rise and the Oman ophiolite. *Journal of the Geological Society, London* **349**, 261–272.

McCollom, T. M. & Shock, E. L. (1998). Fluid–rock interactions in the lower oceanic crust: thermodynamic models of hydrothermal alteration. *Journal of Geophysical Research* **103**, 547–575.

McCulloch, M. T., Gregory, R. T., Wasserburg, G. J. & Taylor, H. P. (1981). Sm–Nd, Rb–Sr and 18O/16O isotopic systematics in an oceanic crustal section: evidence from the Samail ophiolite. *Journal of Geophysical Research* **86**(B4), 2721–2735.

Mevel, C., Gillis, K. M., Allan, J. F. & Meyer, P. S. (eds) (1996). *Proceedings of the Ocean Drilling Program, Scientific Results, 147*. College Station, TX: Ocean Drilling Program.

Nehlig, P. & Juteau, T. (1988). Flow porosities, permeabilities and preliminary data on fluid inclusions and fossil thermal gradients in the crustal sequence of the Sumail ophiolite (Oman). *Tectonophysics* **151**, 199–221.

Nehlig, P., Juteau, T., Bendel, V. & Cotten, J. (1994). The root zone of oceanic hydrothermal systems: constraints from the Samail ophiolite (Oman). *Journal of Geophysical Research* **99**, 4703–4713.

Nicolas, A. & Boudier, F. (1991). Rooting of the sheeted dyke complex in Oman ophiolite. In: Peters, Tj., Nicolas, A. & Coleman, R. (eds) *Ophiolite Genesis and Evolution of the Oceanic Lithosphere*. Dordrecht: Kluwer Academic, pp. 39–54.

Nicolas, A. & Ildefonse, B. (1996). Flow mechanism and viscosity in basaltic magma chambers. *Geophysical Research Letters* **23**(16), 2013–2016.

Nicolas, A., Ceuleneer, G., Boudier, F. & Misseri, M. (1988). Structural mapping in the Oman ophiolites: mantle diapirism along an ocean ridge. *Tectonophysics* **151**, 27–56.

Nicolas, A., Boudier, F., Ildefonse, B. & Ball, E. (2000). Accretion of Oman and United Arab Emirates ophiolite—discussion of a new structural map. *Marine Geophysical Research* **21**(3–4), 147–179.

Nicolas, A., Boudier, F., Michibayashi, K. & Gerbert-Gaillard, L. (2001). Aswad massif (United Arab Emirates), archetype of the Oman–UAE ophiolite belt. *Geological Society of America Bulletin* **349**, 499–451.

Nicolas, A., Mainprice, D. & Boudier, F. (2003). High temperature seawater circulation through the lower crust of ocean-ridges—a model derived from the Oman ophiolites. *Journal of Geophysical Research on line first*. http://www.agu.org/pubs/current/jb/, **108**(B8), 2372.

Pallister, J. S. & Hopson, C. A. (1981). Samail ophiolite plutonic suite: field relations, phase variation, cryptic variation and layering, and a model of a spreading ridge magma chamber. *Journal of Geophysical Research* **86**, 2593–2644.

Phipps Morgan, J. & Chen, J. Y. (1993). Dependence of ridge-axis morphology on magma supply and spreading rate. *Nature* **364**, 706–708.

Pin, C., Briot, D., Bassin, C. & Poitrasson, F. (1994). Concomitant extraction of Sr and Sm–Nd for isotopic analysis in silicate samples based on specific extraction chromatography. *Analytica Chimica Acta* **298**, 209–217.

Rothery, D. A. (1983). The base of a sheeted dyke complex, Oman ophiolite: implications for magma chambers at oceanic spreading axes. *Journal of the Geological Society, London* **140**, 287–296.

Spear, F. S. (1981). An experimental study of hornblende stability and compositional variability in amphibolite. *American Journal of Science* **281**, 697–734.

Spulber, S. D. & Rutherford, M. J. (1983). The origin of rhyolite and plagiogranite in oceanic crust: an experimental study. *Journal of Petrology* **24**, 1–25.

Stakes, D. S. (1991). Oxygen and hydrogen isotope compositions of oceanic plutonic rocks; high-temperature deformation and metamorphism of oceanic layer 3. In: Taylor, H. P., O'Neil, J., *et al.* (eds) *Geochemical Society, Special Publication* **3**, 77–90.

Stakes, D. S. & Taylor, H. P. (1992). The northern Samail ophiolite: an oxygen isotope, microprobe, and field study. *Journal of Geophysical Research* **97**(B5), 7043–7080.

Staudigel, H., Davies, G. R., Hart, S. R., Marchant, M. & Smith, B. M. (1995). Large scale isotopic Sr, Nd and O isotopic anatomy of altered oceanic crust: DSDP/ODP sites 417/418. *Earth and Planetary Science Letters* **130**, 169–185.

Turner, F. J. & Verhoogen, J. (1960). *Igneous and Metamorphic Petrology*. New York: McGraw–Hill, 694 pp.

Wilcock, W. S. D. & Delaney, J. R. (1996). Mid-ocean ridge sulfide deposits: evidence for heat extraction from magma chambers or cracking fronts? *Earth and Planetary Science Letters* **145**, 49–64.

Witt, G. & Seck, H. A. (1989). Origin of amphibole in recrystallized and porphyroclastic mantle xenoliths from Rhenish massif: implications for the nature of mantle metasomatism. *Earth and Planetary Science Letters* **91**, 327–340.